REPORT DOCUMENTATION PAGE

Form Approved
OMB No. 0704-0188

1. REPORT DATE *(DD-MM-YYYY)*	2. REPORT TYPE	3. DATES COVERED *(From - To)*
15-04-2004	Thesis Paper	

4. TITLE AND SUBTITLE
Expanding a Flutter Envelope Using Data from Accelerating Flight: Application to the F-16 Fighter Aircraft

5a. CONTRACT NUMBER

5b. GRANT NUMBER

5c. PROGRAM ELEMENT NUMBER

6. AUTHOR(S)
Charles A. Harris

5d. PROJECT NUMBER

5e. TASK NUMBER

5f. WORK UNIT NUMBER

7. PERFORMING ORGANIZATION NAME(S) AND ADDRESS(ES)

412 TW/ENTT
307 E Popson Ave
Edwards AFB CA 93524

8. PERFORMING ORGANIZATION REPORT NUMBER

PA-04062

9. SPONSORING / MONITORING AGENCY NAME(S) AND ADDRESS(ES)
412 TW/ENTT
307 E Popson Ave
Edwards AFB CA 93524

10. SPONSOR/MONITOR'S ACRONYM(S)

11. SPONSOR/MONITOR'S REPORT NUMBER(S)

12. DISTRIBUTION / AVAILABILITY STATEMENT
A Approved for public release; distribution is unlimited.

20041028 151

13. SUPPLEMENTARY NOTES
CA: Air Force Flight Test Center Edwards AFB CA CC: 012100

14. ABSTRACT Due to the destructive nature of flutter, flutter testing is a mandatory requirement for certification of both civilian and military aircraft. However, along with the complexity of newer aircraft, the time and cost associated with flutter testing has increased dramatically. Considering that many of the test techniques and analysis methods used to perform flutter testing date back to the 1950s and 1960s it may be time to take a fresh look at how flutter testing can best be accomplished.

This thesis revisits flutter testing techniques and proposes an alternative to traditional flutter testing. The alternative uses flight test data from an aircraft that is performing an acceleration to clear the flutter envelope of the aircraft. Four academic issues arise from this new test approach.

(1) Are frequencies and damping affected by the acceleration of the aircraft? (2) Can parameter identification algorithms extract frequency and damping values from the time varying data? (3) Can the vibration response at airspeeds (or Mach numbers) beyond which the aircraft has accelerated be anticipated? (4) What formal criteria can be used to determine when the aircraft needs to end the acceleration and terminate the test point?

The academic contribution of this thesis is to address these issues.

15. SUBJECT TERMS
Aeroelasticity Flutter Limit Cycle Oscillation F-16
Aerodynamics Fluid Structure Interaction Flight Test Modeling and Simulation

16. SECURITY CLASSIFICATION OF:			17. LIMITATION OF ABSTRACT	18. NUMBER OF PAGES	19a. NAME OF RESPONSIBLE PERSON
a. REPORT	b. ABSTRACT	c. THIS PAGE			Charles A. Harris
UNCLASSIFIED	UNCLASSIFIED	UNCLASSIFIED	Unclassified Unlimited	136	19b. TELEPHONE NUMBER *(include area code)* 661-277-3737

Expanding a Flutter Envelope Using Data from Accelerating Flight:

Application to the F-16 Fighter Aircraft

by

Charles A. Harris

B.S., LeTourneau University, 1984

M.S. California Polytechnique University, Pomona, 1990

A thesis submitted to the

Faculty of the Graduate School of the

University of Colorado in partial fulfillment

for the requirement for the degree of

Doctor of Philosophy

Department of Aerospace Engineering

2004

This thesis entitled:

Expanding a Flutter Envelope Using Data from Accelerating Flight:

Application to the F-16 Fighter Aircraft

Written by Charles A. Harris

Has been approved for the Department of Aerospace Engineering

Prof. Charbel Farhat

Prof. Mark Balas

Date_____

The final copy of this thesis has been examined by the

signatories, and we find that both the content and the form

meet acceptable presentation standards of scholarly work

in the above mentioned discipline.

Harris, Charles Allen (Ph.D. Engineering Department of Aerospace Engineering)

Harris, Charles Allen (Ph.D. Engineering Department of Aerospace Engineering)

Expanding a Flutter Envelope Using Data from Accelerating Flight: Application to the F-16 Fighter Aircraft

Thesis directed by Professor Charbel Farhat

Due to the destructive nature of flutter, flutter testing is a mandatory requirement for certification of both civilian and military aircraft. However, along with the complexity of newer aircraft, the time and cost associated with flutter testing has increased dramatically. Considering that many of the test techniques and analysis methods used to perform flutter testing date back to the 1950s and 1960's it may be time to take a fresh look at how flutter testing can best be accomplished.

This thesis revisits flutter testing techniques and proposes an alternative to traditional flutter testing. The alternative uses flight test data from an aircraft that is performing an acceleration to clear the flutter envelope of the aircraft. Four academic issues arise from this new test approach.

1) Are frequencies and dampings affected by the acceleration of the aircraft?
2) Can parameter identification algorithms extract frequency and damping values from the time varying data?
3) Can the vibration response at airspeeds (or Mach numbers) beyond which the aircraft has accelerated be anticipated?
4) What formal criteria can be used to determine when the aircraft needs to end the acceleration and terminate the test point?

The academic contribution of this thesis is to address these issues. It is shown that although the frequencies and damping values do change the change is so small that it is irrelevant. It is also shown that by taking small windows of data, within which the change in parameters is small, it is possible to accurately identify parameters from the time varying data. Finally it is shown that at least in principal parameters can be predicted using data from sub-critical airspeeds, and that testing can be discontinued before an unstable flight condition is reached.

List of Figures

List of Tables

1.0 Justification

Flutter testing is both hazardous and expensive, but it is required to verify that the flutter boundary lies outside of the operational envelope. It is imperative that this testing is accomplished before a new aircraft design is released to an unsuspecting operational pilot. In this chapter, the history of flutter (and other aeroelastic phenomenon) will be reviewed and a summary of the popular test techniques will be presented. Fiscal factors and future requirements that will force flutter testing to be accomplished more efficiently than is currently possible will also be examined. Finally a new test methodology that utilizes vibration response data collected during a longitudinal acceleration to define the frequency and damping profile within the operational envelope will be explored.

The objective of this research is to develop a test methodology that will reduce test cost by simultaneously reducing the number of flight hours, and reducing the calendar time required for accomplishing flutter testing.

The test methodology being developed is designed to replace the traditional flutter clearance methodology for at least the more benign parts of the envelope. Traditionally, flutter clearance is accomplished by first trimming the aircraft at a predetermined flight condition. A forced excitation of the aircraft structure is then initiated, and the forced inputs and responses are measured. The data are analyzed in order to determine the stability of the aircraft structure, and a decision is made whether or not it is safe to continue to the next test point. This process is expensive and time consuming, and is the motivation for this research.

Following is a short introduction of flutter and traditional flutter test techniques that is presented in order to better draw a contrast between the traditional method and the "accelerated flutter test" technique that is the subject of this thesis.

1.1 Description of Flutter

Flutter is an instability caused by the interaction between aerodynamic forces and the elastic structure.

The key words/phrases in this definition are, instability, interaction, aerodynamic forces, and elastic structure.

Starting with the last and working forward, first consider the elastic structure. The linear elastic structure has mass, stiffness, and damping so you can think of the system as an oscillator. The structure is often represented mathematically as:

$$M\ddot{x} + D\dot{x} + Kx = 0 \qquad (1.1)$$

where M is the mass matrix, D is the damping matrix, K is the stiffness matrix, x is the displacement vector, and a dot above a variable represent differentiation with respect to time. This is also known as the dry structure, or the structure on the ground (i.e. without airflow). This is because aerodynamic ("fluid") forces are not acting on it.

Next consider the aerodynamic forces. That is the force that the air exerts on the structure as it rushes past. Mathematically the aerodynamic force can be considered a forcing function on the dry structure. So equation (1.1) becomes

$$M\ddot{x}+D\dot{x}+Kx=F(t) \qquad (1.2)$$

Where F(t) is the time dependent aerodynamic force, and t is the variable time.

There is an interaction between the aerodynamic forces and the structure because the aerodynamic force is dependent on the motion of the structure and the motion of the structure is driven by the aerodynamic force. Mathematically the aerodynamic dependence on the motion of the structure can be expressed as

$$F(t)=\lambda F_M\ddot{x}+\lambda F_D\dot{x}+\lambda F_K x+F_T(t) \qquad (1.3)$$

Where λ is the dynamic pressure, F_M, F_D, and F_K, are matrices representing aerodynamic operators, and F_T represents unsteady aerodynamic forces which are independent of the aircraft motion. An example of a force that would be included in F_T is the unsteady force due to pressure fluctuations induced by high angle of attack. Combining equations (1.2) and (1.3) yields:

$$M\ddot{x}+D\dot{x}+Kx=\lambda F_M\ddot{x}+\lambda F_D\dot{x}+\lambda F_K x+F_T(t) \qquad (1.4)$$

Next move the terms that are dependent on the motion of the structure to the left hand side of the equation.

$$\left(M-\lambda F_M\right)\ddot{x}+\left(D-\lambda F_D\right)\dot{x}+\left(K-\lambda F_K\right)x=F_T(t) \qquad (1.5)$$

In equation (1.5) it is easy to see the dynamic pressure (speed of the aircraft) plays a significant role in the mass, damping, and stiffness of the system. This is what is called the wet structure.

Furthermore it is easy to imagine a case where damping for at least one mode in this system could be driven to instability by the aerodynamic force acting on the structure. In the case where this instability manifests itself the aircraft is said to flutter. For more information on classical flutter development see references [2,28,29,31].

In order to illuminate the differences between traditional flutter testing and the new method being examined in this work, this chapter will present a brief history of flutter (in section 1.2), review the traditional flutter testing methodology and cost (in sections 1.3, and 1.4 respectively), and explore manufacturing developments that will make it difficult to utilize the traditional approach in the future (in section 1.5). Finally this chapter will present the objectives of this research (in section 1.6).

1.2 A History of Flutter

Aeroelastic problems date back as far as four centuries ago, to the windmills in Holland. The spars that were located at the mid-chord were moved to the quarter-chord to prevent twisting. Also some 19^{th} century bridges were weak in torsion and were destroyed by aerodynamic effects. For more on the history of flutter see [1].

The first occurrence of an aeroelastic instability of an aircraft was actually before the Wright brothers first flew. Samuel Langley launched his monoplane from a houseboat in the Potomac River and suffered a structural failure due to divergence. Although divergence is not flutter, it is closely related. In fact a flutter analysis will give the divergence speed at zero frequency. So divergence can be thought of as zero frequency flutter.

During World War I the Handley Page bomber had a control surface flutter problem that was described as a coupling between the aft fuselage and antisymetric elevator motion. As a result of this

and similar problems of the DH-9 in 1917 aircraft designs began to incorporate a stiff torque tube connecting the elevators so the frequency of the antisymmetric elevator mode would be much higher than the torsional mode for the fuselage.

In 1925 two aircraft designs, the Gloster Grebe and the Gloster Gamecock, were found to be unstable due to wing aileron flutter. The problem was fixed by changing the shape of the aileron. Effectively the mass of the aileron was moved forward. More recently using balance weights to move the center of gravity of the aileron has alleviated this type of flutter simply.

The first use of a scaled model to determine the critical flutter speed (the lowest speed at which flutter onset can occur) was 1928. A one third scale model with the same mass density and one ninth the stiffness was used, and the resulting flutter speeds and frequencies of the model correlated well with those of the full scale aircraft.

Many flutter incidences in the late 1920s and early 1930s involved air racers. One account, in 1934, the pilot repeatedly encountered wing-tip flutter. Each time he reduced the wingspan by cutting off the tip of the wing. Eventually the wing area was reduced from 78 square feet to 42 square feet, but the airplane was then flutter-free.

Von Schlippe was the first to accomplish systematic flutter flight-testing in 1935. Prior to this time flutter flight-testing consisted of diving the aircraft to its maximum velocity and hoping for the best. By the late 1940s systematic flight flutter testing had gained wide acceptance in the industry. The first attempt to use a flutter model to simulate free flight conditions was attempted in 1944.

The first example of panel flutter occurred during development of the V-2 rocket between 1942 and 1944. Panel flutter depends on many parameters, which include Mach number and boundary layer, but is especially sensitive to any thermal or compressive effects that tend to create local buckling in the skin.

During flight-testing of the P-80 aircraft, in 1944, a type of flutter called aileron buzz was encountered. This phenomenon is a single-degree-of-freedom form of flutter caused by the coupling of aileron rotation and chordwise motion of shock waves on the wing.

Propeller whirl flutter is suspected in two fatal crashes of the Lockheed Electra turboprop transports. Propeller whirl flutter involves the gyroscopic precession of a flexibly mounted engine-propeller system. It was first explored academically in 1938, but was thought to be only of academic interest until the Electra crashes in 1959.

1.3 Flutter Test Techniques

Flutter testing can be decomposed into four areas; 1) excitation type, 2) excitation method, 3) response measurement, and 4) data analysis. The capabilities and limitations of the techniques used to accomplish these four areas have driven flutter flight test engineers to the usual flutter testing techniques that have been used for decades.

The usual method used for flutter testing aircraft is to fly stabilized test points at predetermined conditions. For example, to clear the aircraft at 10,000 feet for a given configuration, it may be necessary to conduct stabilized test points at eight to twelve speeds at that altitude. After the first two or three test points are accomplished within the analytically cleared envelope, the damping trend is extrapolated and a determination is made whether or not it is safe to continue to the next test point. If it is safe to go to the next test point, the process is continued until the top speed for that altitude is achieved. It is easy to see, if several configurations have to be cleared at several altitudes the full test matrix becomes very time consuming and expensive. For more information on flutter flight test procedures see references [24,26,30,36].

1.3.1 Excitation Type

Excitation type describes the input signal that generates the vibration response of the airframe. The excitation types that are commonly used are decay, impulse, harmonic excitation (sine dwell), sine sweep, tailored inputs, and random inputs. For more information on excitation types see references [37,38,39].

1.3.1.1 Decay Data

Decay data are what you get in the absence of an excitation signal. Typically the aircraft structure is excited by some other type of excitation after which the excitation is abruptly halted. The data are recorded and analyzed for the period after the excitation has been halted.

1.3.1.2 Impulse Excitations

Impulse excitations are typically used as a method to generate decay data. Striking the control stick with a hand or a mallet, kicking the rudder, or detonating pyrotechnic charges located on the wing of the aircraft, can produce the impulse. Striking the control stick with a hand or kicking the rudder cannot adequately excite structural modes with frequencies higher than about 5 – 6 Hz. Figure 1.1 shows a typical impulse excitation along with the decay response.

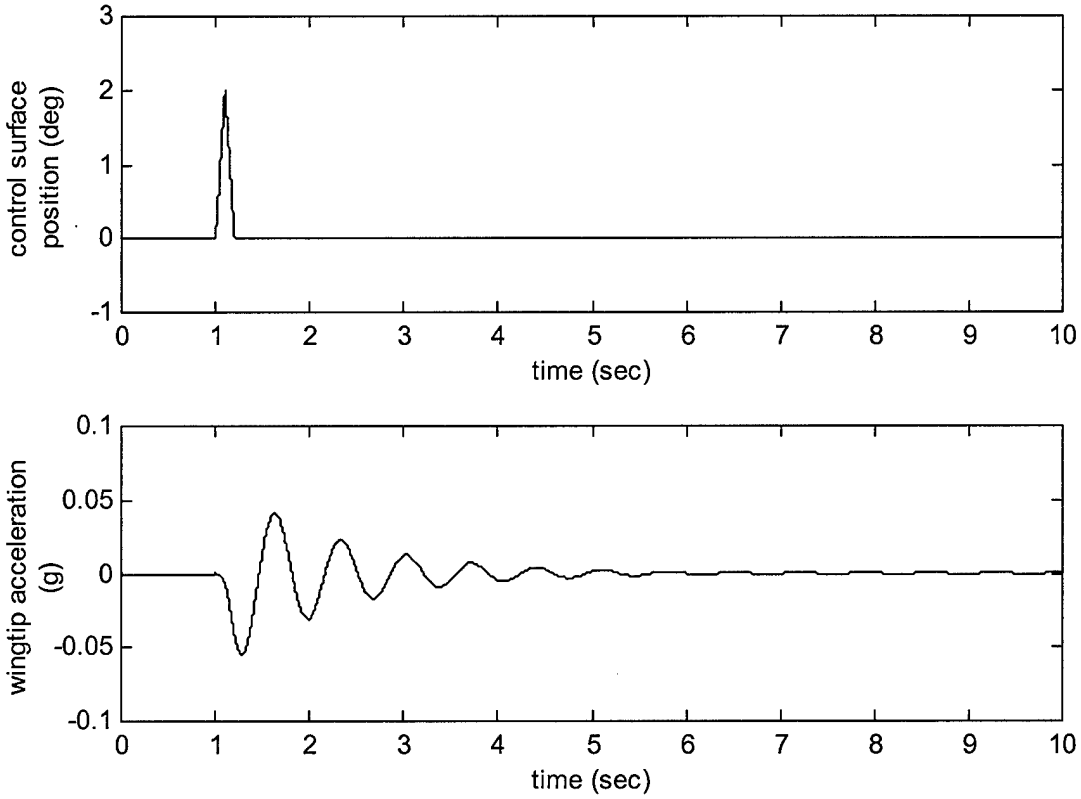

Figure 1.1: Typical impulse excitation and decay response

1.3.1.3 Harmonic Excitations

Harmonic excitation (sine dwell) is a sustained sinusoidal signal that is tuned to the harmonic frequency to be excited. This excitation is useful because it typically excites only one mode, and it puts more energy into that one mode. Unlike decay data and impulse data, harmonic data are typically recorded during the excitation and therefore the analysis methods should account for the driving force.

1.3.1.4 Sine Sweep

Sine sweep is similar to sine dwell except the frequency of the sine wave is varied with time. Sometimes the variation is linear and sometimes the variation is exponential. The exponential sine

sweep is normally preferred because it puts an equal amount of energy into each frequency. Figure 1.2 shows a typical sine sweep. In this case the frequency varies linearly with time.

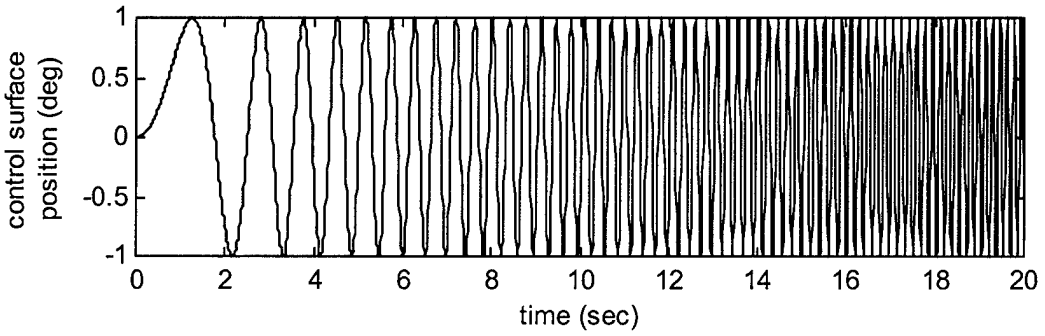

Figure 1.2: Typical sine sweep using linear variation in frequency.

1.3.1.5 Tailored Inputs

Tailored inputs focus energy on predetermined frequency bands. These are of academic interest, however, they are not used much in practice because they require knowing the frequencies of the system under test in advance.

1.3.1.6 Random Inputs

Random inputs use a pseudo-random signal to excite the structure of the aircraft. This can be a very quick way to identify the structure, however the energy is spread across a wide spectrum and may not adequately excite modes.

1.3.2 Excitation Methods

Excitation methods that are commonly used fall into three categories; 1) aerodynamic methods, 2) moving mass methods, and 3) pyrotechnic methods. The aerodynamic methods are control surface excitation, oscillating vane excitation, and random turbulence excitation. The moving mass methods include inertial excitation and electrodynamic excitation. Pyrotechnics methods use small explosive charges to generate an excitation. Sometimes these pyrotechnic devices are called bonkers. For more information on excitation methods see references [37,38,39].

1.3.2.1 Aerodynamic Excitation Methods

The first of the aerodynamic methods used to excite the aircraft structure is control surface excitations. Control surface excitations can be pilot induced or flutter excitation system induced. Pilot induced excitations are low quality, unrepeatable, and normally contain only frequencies below 5 – 6 Hz. Flutter excitation systems are capable of producing repeatable signals with any frequency content the aircraft is capable of producing.

Oscillating vane excitations can be produced by an airfoil or slotted tubes. The airfoil can produce any type of excitation, but the slotted tubes can only produce sine dwell and sine sweep excitations. The slotted tubes also have a tendency to get stuck due to aerodynamic stresses in the tubes. Figure 1.3 shows a typical aerodynamic vane excitation system that utilizes airfoils to produce an excitation force.

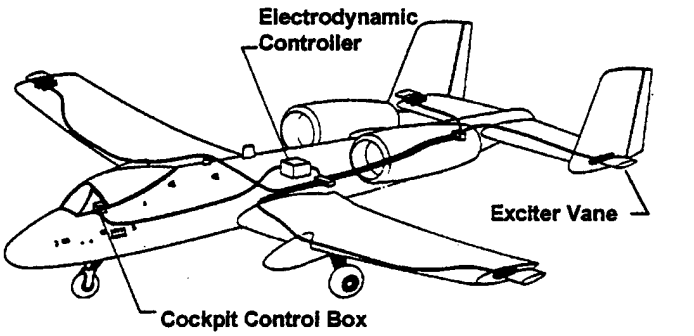

Figure 1.3: Aerodynamic excitation system utilizing oscillating airfoils to produce an excitation force

Random turbulence excitation is the polite name for flying around looking for gusts. This method is only used when there is no alternative (i.e. the program cannot afford to properly instrument the aircraft, or when the aircraft excitation system cannot excite the frequency of concern). The signal to noise ratio is very low for this type of data so the data have to be averaged. Care must be taken to assure that the data that are averaged is in phase. This can be done using an algorithm called random decrement if there are only one or two dominate modes in the data. The random decrement algorithm is basically a triggering technique. Data are collected from the time the trigger is tripped for a predetermined number of samples. Filters are sometimes used to assure there will only be one or two modes in the data. After the resulting data are averaged it is treated like decay data.

1.3.2.2 Moving Mass Excitation Methods

Moving mass methods include inertial excitation, another name for an unbalanced mass. An unbalanced mass spinning on a shaft creates an oscillating force on the structure. Unless the mass can

be moved the force increases as the shaft rotates faster. This results in a system that has a small frequency range in which it is effective. This is typically a low budget approach to flight-testing. If the program can afford it, it is better to use one of the aerodynamic methods discussed above with the exception of random turbulence.

Electrodynamic excitation is similar to the unbalanced mass except the mass is driven by an electrodynamic shaker. This is the excitation method that was used on the B-1B flutter envelope expansion. Figure 1.4 shows a cartoon of the inertial shaker system that was used on the B-1B. The benefits of using this method include good frequency range, measurable input force, and repeatable execution. The primary drawback is the mass required to generate a suitable force on the structure can change the modal characteristics.

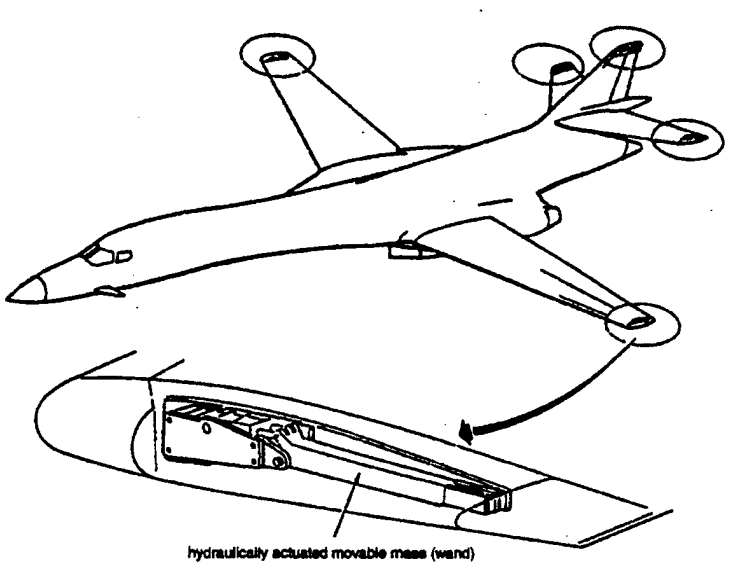

Figure 1.4: Inertial excitation system used on the B-1B

1.3.2.3 Pyrotechnic Excitation Methods

Bonkers are not used in the United States because of Safety of Flight considerations. However, Europe has a slightly different philosophy that allows the use of pyrotechnics. The bonkers produce a nice impulse force with good frequency content, and they can be detonated together to excite a particular mode. The only problems with the bonkers are the safety implications and the number of test points that can be accomplished in one mission is determined by the number of bonkers that can be attached to the wings.

1.3.3 Response Measurement

There are only two kinds of sensors that are typically used to measure the response of the system. Accelerometers are used wherever the displacements tend to be large (e.g. wing tips), and strain gauges are used where the strain tends to be large (e.g. wing root). Experience suggests the accelerometer data are the best suited for identifying frequency and damping. Typical sample rates for flutter data range from 100 Hertz to 800 Hertz. For more information on response measurement and how the data is transmitted to the control room see references [32,33,34,35].

1.3.4 Data Analysis

There are several techniques widely used for analyzing flutter test data. The selection of analysis technique is highly dependent on the excitation method that is used. Some of the common data analysis techniques are half power, time history curve fit, frequency curve fit, random decrement, pseudo-random decrement, and log decrement. For more information on data analysis methods see references [40,41,42].

1.3.4.1 Half Power Analysis

Half power uses the width of the modal lobe at the half power line of the Power Spectral Density (PSD), the auto-spectrum or the Fast Fourier Transform (FFT), to determine the damping value for that particular mode. Figure 1.5 shows how the half power line is defined for the power spectral density or an auto-spectrum (cases where the amplitude has squared units). Figure 1.6 shows how the half power line is defined for an FFT (cases where the amplitude does not have squared units). Once the lobe width at the half power line is determined as in equation () then the damping can be determined using equation (). This technique is highly dependent on the analyst and it becomes significantly less reliable when considering closely spaced modes. This is particularly problematic because two closely spaced modes are often an indication of impending flutter conditions. The advantage of the half power analysis technique is, it can be used with most data collection methods. However this flexibility comes at the cost of confidence in the results.

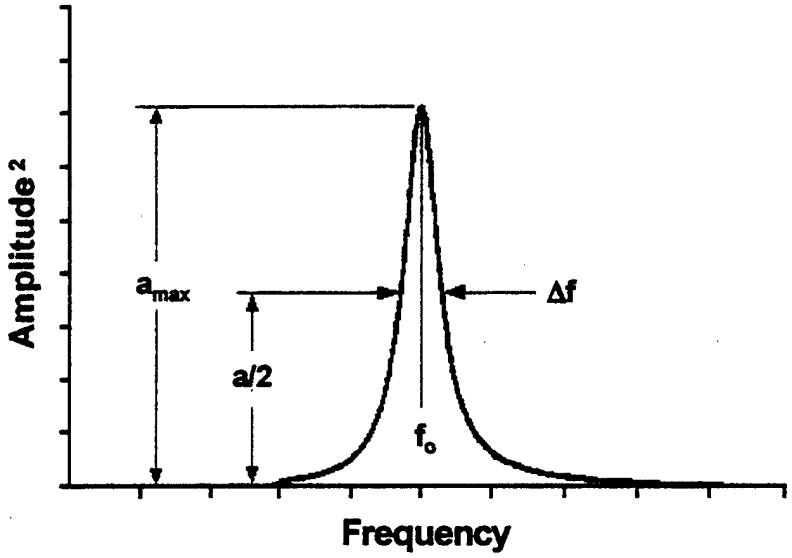

Figure 1.5: Half power method for Power Spectral Densities and Auto spectrum.

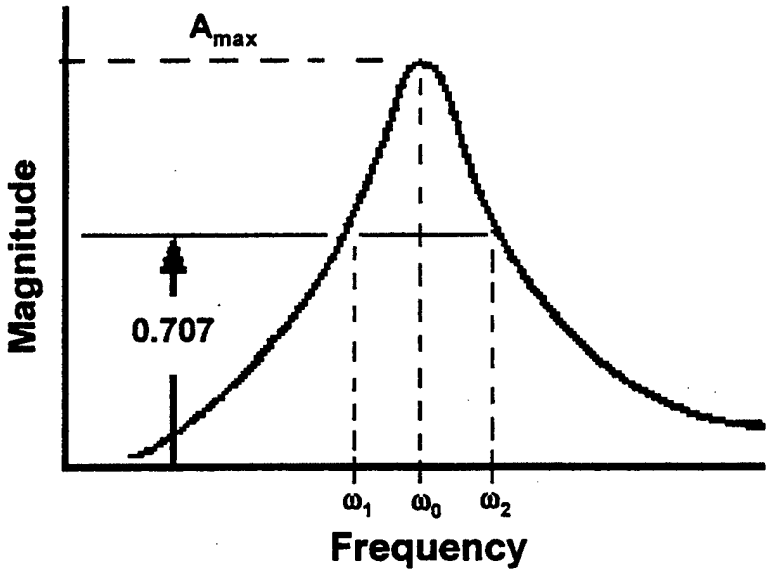

Figure 1.6: Half power method for Fast Fourier Transforms.

$$\Delta F = F_{hi} - F_{lo} = \omega_2 - \omega_1 \quad (1.6)$$

$$\zeta = \frac{\omega_2^2 - \omega_1^2}{4\omega_0^2} \quad (1.7)$$

1.3.4.2 Log Decrement Analysis

Log decrement uses decay data to assess the damping of the mode of interest taking advantage of the relationship between the damping value and the number of cycles (N) it takes for the amplitude of the mode at time zero (A_0) to be reduced to some fractional value (A_N). Equation (1.8) gives the algorithm that is used to determine damping from the decay data. Sometimes, in order to expedite the estimation of damping, equation (1.9) is used. In equation (1.9) $N_{1/2}$ is the number of cycles it takes

to reduce the amplitude to $A_0/2$. Sometimes band pass filtering is used to isolate modes. Log decrement offers consistent results, and is much less dependent on the analyst than half power. However, like half power, it is not very effective when dealing with closely spaced modes. This method is also limited to decay data, which does not always contain the modal energy necessary to achieve accurate results.

$$\zeta = \ln(A_0 / A_N)/(2\pi N) \quad (1.8)$$

$$\zeta = 0.11/N_{1/2} \quad (1.9)$$

1.3.4.3 Time History Curve Fit Analysis

Time history curve fit is a least squares curve fit of the time history data that assumes an underlying function comprised of damped sinusoids (Equation (1.10) gives the general form of the assumed function for time history curve fit).

$$y(t) = C + \sum_{n=1}^{N} A_n e^{\zeta_n f_n t} \sin(f_n t + \varphi_n) \quad (1.10)$$

Where:

A_n	=	maximum amplitude of mode n
C	=	zero offset correction
t	=	time in seconds
$y(t)$	=	value of signal at time t
N	=	maximum mode number
φ_n	=	phase angle of mode n in radians

f_n = natural frequency of mode n in radians/second, and

ζ_n = damping ratio of mode n

The method iteratively improves the damping estimate and then the frequency estimate. The method requires an a priory estimate of the frequency which is normally accomplished by using a Fast Fourier Transform of the flight test data. Because it assumes damped sinusoids this method is only useful for decay data. When this method converges to a solution it provides consistent and accurate results.

1.3.4.4 Frequency Curve Fit Analysis

Frequency curve fit is a least squares curve fit of the cross spectrum of the flight test data that assumes an underlying function that is the ratio of complex polynomials which is shown in equation ().

$$G(j\omega) = \frac{p_0 + p_1(j\omega) + p_2(j\omega)^2 + \cdots}{1 + q_1(j\omega) + q_2(j\omega)^2 + \cdots} = \frac{P(j\omega)}{Q(j\omega)}$$

$$= \frac{(p_o - p_2(\omega)^2 + p_4(\omega)^4 \cdots) + j\omega(p_1 - p_3(\omega)^2 + p_5(\omega)^4 \cdots)}{(1 - q_2(\omega)^2 + q_4(\omega)^4 \cdots) + j\omega(q_1 - q_3(\omega)^2 + q_5(\omega)^4 \cdots)}$$

$$= \frac{\alpha + j\omega\beta}{\sigma + j\omega\tau} \approx F(j\omega) = R(\omega) + jI(\omega)$$

Where:

$G(j\omega)$ =approximating function representing the transfer function

$p's$ =unknown numerator coefficients to be solved for

$q's$ =unknown denominator coefficients to be solved for

$F(j\omega)$ =cross spectrum of the flight test data which approximates the transfer function

$R(\omega)$ =real part of $F(j\omega)$

$I(\omega)$ =imaginary part of $F(j\omega)$

The damping and frequency values can be calculated from the roots of the denominator, which give the poles of the system. This method requires the interaction of the analyst, and two to four minutes worth of data. This method is only useful when an excitation system is used to excite the structure. For more on this analysis technique see references [22,23].

1.3.4.5 Random Decrement Analysis

Random decrement is not an analysis technique as much as it is a preconditioner. This technique is used on random turbulence data in order to average out the unwanted signal. It works by taking a block of data starting at the point the amplitude of the data crosses a trigger value that is set by the analyst. In the end all of the blocks of data are averaged. The resulting signal is referred to as the randomdec signature. The randomdec signature can then be used with any analysis technique that utilizes decay data. Typically this technique is used in conjunction with the log decrement method. This technique typically requires several minutes of flight test data to achieve results. For more detailed information regarding random decrement analysis see reference [25].

1.3.4.6 Psudo-Random Decrement Analysis

Psudo-random decrement is much like the random decrement method. In this case an excitation system is used to induce vibration into the structure, then the excitation system is abruptly halted. Instead of using a trigger level to determine when the blocks of data are started, this technique starts the block of data a few samples after the excitation system is halted. This method can identify a single

mode of interest using data from a few excitations. The total elapsed time necessary to collect the data from these excitations is about 15 to 30 seconds. This is a very useful method as long as there are only one or two modes of interest.

1.4 Cost of Flutter Testing

The F-16 Block 60 program will be used as an example of the cost of flight testing, and the potential benefit of using the flight test and simulation techniques described in this thesis. The F-16 Block 60 is a significant modification to the current F-16 that is being produced by Lockheed Aircraft for sale to the United Arab Emirates. Structurally the Block 60 will not change much, however, the surface geometry will change somewhat in order to increase the fuel capacity. Barring unexpected complications, flutter clearance will be straightforward. However, this program intends to certify 1500 weapons configurations including fully loaded configurations, as well as configurations that occur as a result of selectively dispensing weapons. Using current methods, only the 10%, or 150 loads that are both stable and easily simulated, can be cleared using simulation. For example low subsonic conditions with lightweight and stable stores. The rest (1350 loads) should be cleared through flight test. I say should be cleared through flight test because it is prohibitive to do this much flutter clearance work for a single program. In reality what would happen is the program will assume more risk by choosing what is believed to be the worst case loads and leaving many loads untested even though these loads are potentially hazardous. Therefore the benefits improving the efficiency of the flutter clearance process will be a combination of cost avoidance and risk reduction.

The analysis presented below is an attempt to quantify the benefits.

Starting with the requirements to test without clearing the configuration using accelerating flight-test data, or coupled field analysis, 1350 configurations must be cleared using flight test. Normally it would take at least 3 hours to clear one configuration. This analysis will use the condition that each

configuration is cleared, on average, in 2 hours. Therefore testing will take about 2700 hours of flight time.

Traditionally, predictive flutter clearance analysis is done using a structural dynamics, and aerodynamics models that are very low fidelity. It has been necessary in the past to use these low fidelity models due to computational power that was available at the time. Supposing that the cost of doing this traditional analysis is negligible. It is safe to say that the total cost of the flight test program done to completion would be at least $15M.

The lowest rate the Air Force Flight Test Center would charge for flight testing an F-16 aircraft is about $5600 per hour (as of 2001). This rate does not include the control room, range time, telemetry, or a chase aircraft. All of which are required for hazardous flight-testing. The cost of 2700 hours at $5600 per hour is just over $15M. What is worse than the cost, is the schedule impact of doing that much testing. If eight flights per week are flown, and one hour of testing is accomplished during each flight it will take 330 weeks (over 6 years) to complete the flight test program.

Compare the program cost and schedule above to that of using coupled field analysis and data from accelerated flight. If the fidelity of coupled field analysis is such that Limit Cycle Oscillation can be dependably predicted the total number of flight test points that must be flight-tested could be cut by an order of magnitude (or 90%). That means that 150 configuration, would have to be flight-tested. Also, using data from accelerated flight could reduce the number of hours to clear a configuration to one. Therefore it would take 150 flight hours to complete the flight-testing.

Realizing that the complexity per flight hour has increased, allowance needs to be made for the rate to increase. So, for this case the rate of $10,000/hour will be used. Therefore the total cost of the flight test would be $1.5M. Add to that $1M for conducting the simulations. The total cost of the program is $2.5M. The total return would be at least $12.5M.

As far as schedule goes, a more realistic sortie rate of three flights per week will still complete the program in 50 weeks, or less than one year. With these cost and schedule savings, the program could truly clear the entire 1500 configurations, and not risk the lives of operational users, and the program could still come in under cost and schedule.

1.5 New Technologies and Tactics

New technologies such as flexible manufacturing, rapid prototyping, and powder metallurgy will make it practical to build aircraft without going into large-scale production. For example if you want to build one or two of a kind aircraft for a specific mission it will be possible to do that. This is also consistent with some of the conceptual tactics that are starting to surface. It is feasible to counter a handful of fighter designs that are currently in the US arsenal, but if hundreds of fighter designs are available, counter measures become much less tractable. All of this pretty much assures there will be an increased need to do flutter testing in the future. With a shrinking flight test force it will become critical that clearance of the flutter envelope for new aircraft be accomplished more efficiently than ever before. Flutter test techniques that are currently used differ only slightly from the techniques that were used 50 years ago. Computer technology has been used to expedite the data analysis process, but has not been used to expedite the flight test process. This research is focused on using high fidelity simulations in conjunction with a new flight test technique to demonstrate a revolutionary flight test approach capable of achieving the increased efficiency that the future demands.

1.6 Objectives

In the new test methodology the aircraft would stabilize at a low airspeed and predetermined altitude/configuration. While the aircraft maintains altitude, an excitation system would be turned on and the aircraft would begin to accelerate. As the airspeed increases the frequencies and damping

values would continually be calculated and displayed very near real time. The aircraft would continue to accelerate until it reaches a predetermined velocity as long as the analysis indicates it is safe to continue. There are two big advantages to testing using this methodology rather than traditional flutter test methods. The first is simply test efficiency. One altitude/configuration combination could potentially be cleared in a matter of minutes rather than the hours it can take in some cases. The second is the resolution of data. In the traditional approach, damping estimates are only available for the test point conditions that have been accomplished. In the accelerated approach there is a potential that the frequency resolution of the damping curve would be almost continuous.

In order to accomplish this objective there are several issues that must be addressed.

1) The first issue is whether or not the frequencies and dampings are affected by the acceleration of the aircraft.
2) The second issue is whether or not parameter identification algorithms can extract frequency and damping values from the time varying data.
3) The third issue is the need to anticipate the vibration response at airspeeds (or Mach numbers) beyond which the aircraft has accelerated.
4) The fourth issue is developing formal criteria to determine when the aircraft needs to end the acceleration and terminate the test point.

Before these issues are examined in detail, there are certain requirements that must be observed if this research is to become a usable flight test tool. These requirements will be examined in chapter 2.

The first of these issues will be addressed in chapter 3. The typical wing section will be introduced in this chapter, and the effects of acceleration on the typical wing section will be explored analytically. Using the typical wing section, a model will be developed that will approximate the F-16 fighter aircraft. Finally it will be shown that, for this practical case, the effects of the accelerations are negligible.

The second of these issues will be addressed in chapter 4. This chapter will introduce the idea of windowing and its effect on time varying data. A summary will be give of the Eiganvector Realization Algorithm (ERA), and its variant FastERA and the utility of FastERA as a flight test parameter identification tool will be assessed by exploring the effects of window length, sample rate, and noise level on the algorithm. Finally, FastERA is used to identify the frequency and damping modes of the accelerating simulation results for the two degree of freedom model of the F-16 that is developed in chapter 3. The results are compared to the results of an actual F-16 providing validation for both the use of FastERA for accelerating data, and the accuracy of the 2 degree of freedom model.

The results that were obtained from the comparison of frequency and damping values between flight test and the two degree of freedom model of the F-16 convinced the Air Force Flight Test Center (AFFTC) to support a deeper exploration into the feasibility of the accelerated flutter testing approach. The Air Force Test Pilots School, located at the AFFTC flew F-16 test sorties to collect both stabilized and accelerated flight test data for a configuration consistent with 3 dimensional simulations that were being prepared at the University of Colorado. The details of the flight test performed by the Test Pilots School are presented in chapter 5 and the 3 dimensional simulations will be presented in chapter 6.

The third issue, namely "the need to anticipate the vibration response at airspeeds beyond which the aircraft has accelerated", will be addressed in Chapter 7. An analytical study of a one degree of freedom system and a two degree of freedom system is developed. Estimators are developed for these systems, which are shown to be overly conservative. Finally, a symbolic solver is used to get an exact solution.

The final issue, namely "developing formal criteria to determine when the pilot needs to end the acceleration and terminate the test point", is also addressed in chapter 7. Utilizing the solutions for the one and two degree of freedom systems to project the flutter speed, the acceleration can be decreased or stopped when the control room personnel and the pilot have ample time to react.

1.7 Contributions of this Thesis

The contribution of this thesis, to the flight test community, is the development of a new flight test procedure for conducting flutter testing for advanced military aircraft. This new flight test procedure will expedite flight testing by providing a means of conducting flutter tests, and identifying frequency and damping parameters for the critical modes of the aircraft during an accelerated flight.

The proposed flight test technique raises theoretical and algorithmic issues that have not been addressed previously. Specifically, the effect of acceleration on the flutter parameters of the aircraft, whether parameters can be identified using data from an accelerating aircraft, and the real time prediction of the aircraft damping beyond the current airspeed needed to be investigated.

Therefore the contributions of this thesis to the academic community are:

1) The quantification of the effect acceleration has on an aerodynamic system. It was shown that this effect, although real, is not of significant magnitude to invalidate test results.

2) The parameter identification using data from an accelerating aircraft was accomplished using small window sizes within which the parameters do not change significantly. In practice the acceleration of a typical aircraft is not sufficient to alter the results of the parameter estimation within the small window.

3) The use of estimators were employed in order to predict, or extrapolate, the damping characteristics at higher airspeeds, this thesis develops both an estimator and an exact solution for a simplified aeroelastic system found in the classical literature. The estimator was found to be unacceptably conservative, and the exact solution was found to be quite cumbersome even for the simplified system.

However, it is shown, at least in principle, that the accelerated flutter technique is viable.

4) A preliminary design of the criterion to be used to assure that the testing is halted before the aircraft crosses the flutter boundary is developed to support the new flight test technique.

5) Finally, validation is performed, primarily to validate the flight test technique. However, this validation will, as a consequence, validate the simulation technology.

2.0 Requirements for the New Flight Test Technique

2.1 Safety of Test

It is important that any new flight test methodologies maintain, or increase the level of safety provided by the methodologies which they replace. The proposed method of accomplishing parameter identification and clearance to proceed as the aircraft accelerates across an altitude band might seem cavalier at first. However, there are safety advantages to using this methodology. It is a truism that most flight test accidents occur when the aircraft is not performing a test point. It is during this period when the pilot and the control room are more relaxed that mistakes can more easily be made. Therefore there is a safety gain because several stabilized test points are replaced by one accelerating test point.

While conducting flutter testing the data sometimes are difficult to interpret because the resolution of the stabilized test points. For example if a downward trend in damping is expected at a given Mach number, say 0.84 Mach, but in reality the trend starts 0.83 Mach. If you have a data point at 0.80 Mach and 0.85 Mach it will not be clear whether the break occurred at 0.83 Mach or at 0.84 Mach and was much more severe than anticipated. This confusion is compounded by noise in the damping measurement. Instead of points being exactly identified there is some confidence region around the points. In practice when these kinds of uncertainties suggest a potential hazard more test points will be added to better characterize the region. With the proposed methodology the parameter identification would be continuous so there would be another safety gain by using this methodology.

The simulation being used in this research is higher fidelity than has previously been used to support flutter flight tests. These high fidelity simulations alone result in higher confidence in the predictions which subsequently results in a higher level of safety during test.

2.2 Noise Tolerance

There are multiple sources of noise that affect flight test data. First, there is atmospheric turbulence which is not accounted for in most data reduction algorithms. Second, between the engines and the airflow an airplane represents a fairly harsh vibration environment. Third, the input forces cannot be measured directly. Instead the deflection of the control surface is measured. Fourth, all of the usual measurement errors apply to aircraft instrumentation as well.

Because flight test data are inherently noisy, it is critical that any data analysis method that is used is tolerant of noise. In other word the data analysis method must be capable of identifying frequencies and damping values even when there is a high percentage of noise in the data.

2.3 Sample Rate Effects

One method of making algorithms more tolerant of noise is to collect more data. A straight forward way to collect more data is to increase the rate at which the data are sampled. When an algorithm is used that depends on Fourier transforms the increased sample rate results in decreased frequency resolution. This may in turn adversely affect the algorithms ability to correctly identify the frequency and damping values.

There is also a practical limit to the rate at which the data can be sampled and telemetered to the ground. The government continues to sell radio frequencies to private industry. With the proliferation

of wireless technology, bandwidth that has traditionally been used to support flight test telemetry is lost. For this reason, sample rates for flutter testing will likely remain at the current 100 – 800 samples per second.

Therefore it is a requirement that the parameter identification algorithm used can identify frequency and damping values from data at these sample rates.

2.4 Real Time Requirement

It is a requirement that frequencies and damping values be calculated real time as well as predictions and knock-it-off calculations be performed real time. Otherwise, accelerating the aircraft as the flutter analysis is performed would pose too great of a safety risk.

3.0 Effects of Acceleration on Structural Parameters

It is important when considering the use of flight test data from an accelerating aircraft to verify flutter parameters remain essentially the same, as they would be for an aircraft in stabilized flight at the same conditions. For this reason this chapter examines the effects of the acceleration on the flutter parameters. This issue will be investigated by an analytical study. The analytical model depends on the equations of motion that will be presented for a two degree of freedom "typical wing section". Next the equations of motion will be modified to account for the effects of accelerating the frame of reference, which is attached to the fuselage of the aircraft. Finally, these equations will be applied to a two dimensional representation of an F-16 wing, and it will be shown that for an F-16 the effect of acceleration will be negligible. The primary purposes of this chapter are, to quantify the effects of acceleration on the structural parameters, and to demonstrate that those effects are not significant for a realistic aircraft conditions.

3.1 Discrete Equations of Motion

The equations of motion for a typical wing section [2] (see Fig.3.1) in the absence of accelerations can be written as follows.

$$m\ddot{h} + S_\theta \ddot{\theta} + k_h h = Q_h \qquad (3.1)$$

$$S_\theta \ddot{h} + I_\theta \ddot{\theta} + K_\theta \theta = Q_\theta \qquad (3.2)$$

Where:

m	total mass per unit span of the wing
h	bending degree of freedom
θ	torsional degree of freedom
S_θ	$m(x_G + x_C)$ static moment of inertia
I_θ	polar moment of inertia
K_h	bending stiffness coefficient
K_θ	torsional stiffness coefficient
Q_h	resultant aerodynamic force
Q_θ	resultant aerodynamic moment
G	center of gravity
C	center of elasticity

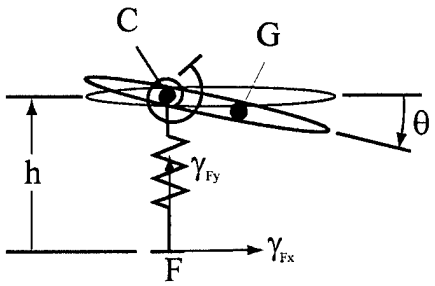

Figure 3.1: A typical wing section: elastic center (C), center of gravity (G), fuselage (F), angle of attack (θ).

Because the reference frame is attached to the aircraft for equations (3.1) and (3.2) inertial terms must be added whenever the aircraft undergoes acceleration at the center of gravity. When the aircraft is accelerating, but θ remains small then the dynamic equations of motion become:

$$m\ddot{h} + S_\theta \ddot{\theta} + k_h h = Q_h^* \qquad (3.3)$$

$$S_\theta \ddot{h} + I_\theta \ddot{\theta} + K_\theta^* \theta = Q_\theta^* \qquad (3.4)$$

Where the inertial terms that result from the acceleration of the aircraft are given by the equations below.

$$K_\theta^* = K_\theta - m\gamma_{F_x}(x_G^0 - x_C^0) - m\gamma_{F_y}(y_G^0 - y_C^0) \qquad (3.5)$$

$$Q_h^* = Q_h - m\gamma_{F_y} \qquad (3.6)$$

$$Q_\theta^* = Q_\theta + m\gamma_{F_x}(y_G^0 - y_C^0) - m\gamma_{F_y}(x_G^0 - x_C^0) \qquad (3.7)$$

Where

F Denotes a fixed point on the fuselage

γ_{F_x} Acceleration in the x (horizontal) direction (note: positive denotes deceleration of the wing section)

γ_{F_y} Acceleration in the y (vertical) direction

The superscript 0 denotes the value at time $t = 0$.

As can be seen from Equations (3.3) and (3.4) above, accelerating the wing section changes both of the aerodynamic forces and the torsional stiffness. These changes are simply the result of inertial forces due to the fact that the equations represent an accelerating system and a frame of reference that is fixed to the aircraft.

The torsional force changes because the center of elasticity and the center of gravity do not coincide. As a result the inertial force acts on this moment arm to produce a torsional force.

If the airfoil rotates, as shown in figure 3.2, from its original position the moment arm changes in length (for small angles of rotation the moment arm changes by $(x_G^0 - x_C^0)\alpha$) resulting in a torsional force that is proportional to the rotational displacement. It is this term, $m\gamma_{F_x}(x_G^0 - x_C^0)$, that is added to the torsional stiffness term, K_θ.

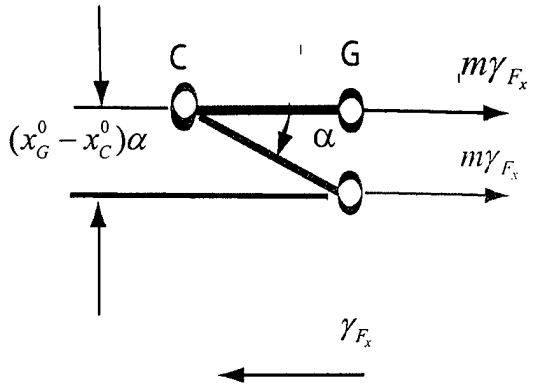

Figure 3.2: Torsional stiffness is affected by acceleration because the inertial force $m\gamma_{F_x}$ acts on the moment arm $(x_G^0 - x_C^0)\alpha$ (for small angles α).

The result, for an aircraft that has a forward acceleration, the stiffness increases if the center of gravity is aft of the center of elasticity due to the term $m\gamma_{F_x}(x_G^0 - x_C^0)$. Similarly, if the aircraft has an upward acceleration component the rotational stiffness will be increased by center of gravity is below the center of elasticity due to the term $m\gamma_{F_y}(y_G^0 - y_C^0)$. However, for level accelerated flight the acceleration rate γ_{F_x} is small (perhaps 0.01 Mach/sec), and the term $(x_G^0 - x_C^0)$ will also be small because x_G^0 and x_C^0 are normally located within one quarter chord of each other. Therefore, for most if not all aircraft the quantity $m\gamma_{F_x}(x_G^0 - x_C^0)$ is negligible. Also for accelerated level flight $\gamma_{F_y} = 0$. Therefore it can be reasonably argued that $K_\theta^* \cong K_\theta$. All other coefficients of the left hand-side of Equations (3.6) and (3.7) are unaffected by the acceleration. Therefore it can be concluded the aeroelastic parameters (i.e. frequency and damping) for level accelerated flight are the same as for accelerated flight conditions.

So to conclude there are some minor effects that acceleration has on the underlying parameters of the system. However, in practice these effects are so small they can be ignored without consequence. Section 3.2 will use an airfoil model that represents an F-16 to demonstrate the acceleration effects can be ignored.

3.2 A Typical (2-D) Wing Section Model for the F-16

This model was developed to match the dynamic characteristics of the F-16. This model will be used to demonstrate the effect of acceleration on the flutter parameters. In chapter 4 simulations will be performed using this model in order to validate the use of ERA and the Accelerated Flutter Test technique.

Starting from a detailed finite element structural model of a "clean" right wing of the F-16 Block 40 equipped with a missile launching system at its tip (Fig. 3.3). The objective is to construct a two-degree of freedom wing section model that is equivalent to the three-dimensional wing in the following sense

1. It reproduces the first bending and torsion frequencies, which are predicted by the three-dimensional finite element model of the wing to be 4.76 Hz and 7.43 Hz, respectively.

2. It reproduces the same bending and torsion modal masses.

3. It reproduces the same vertical displacement at the leading edge of the cross section located at 68% of the distance from the root to the tip of the three-dimensional wing, for both bending and torsion mode shapes, when these are normalized to a unit rotation of the cross section.

When the wing has a large aspect ratio and a small sweep angle, it is commonly suggested to choose the mechanical properties of the typical wing section as to match those of the cross section located at 70% to 75% of the distance from the root to the tip of the three-dimensional wing (for example, see [2] and references 6-1 and 6-2 therein). Nevertheless, the cross-section located at 68% of the distance from the root to the tip (see Fig. 3.3) was chosen, as stated in criterion 3 above, because the F-16 wing is strongly tapered and is rather soft towards its tip.

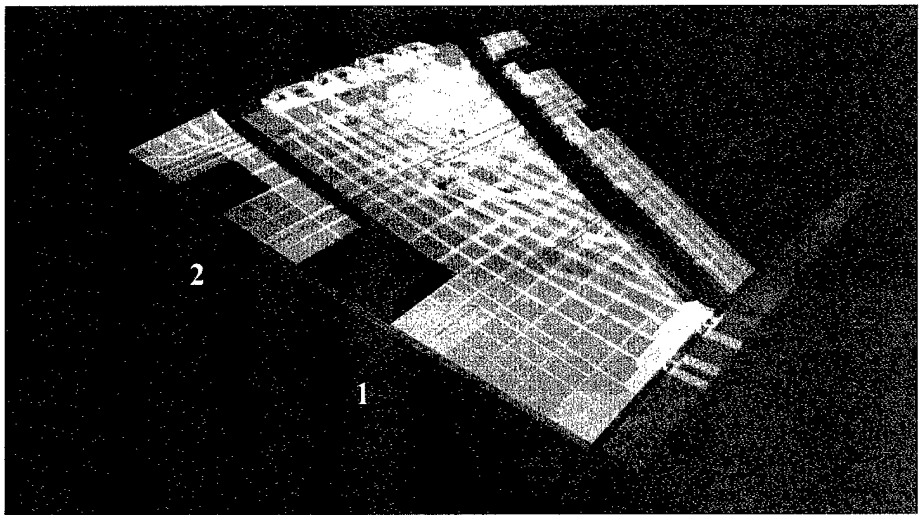

1: cross-section chosen for the structural properties
2: cross-section chosen for the aerodynamic properties

Figure 3.3: Three-dimensional detailed finite element model of an F-16 wing

Besides the shape of the airfoil, six parameters define the sought-after typical wing section, These are denoted collectively by, P_{tws} where the subscript tws stands for typical wing section, and listed below

$$P_{tws} = \{m, I_0, x_G, (x_G - x_C), K_h, K_\theta\} \tag{3.8}$$

The three criteria stated above for establishing the equivalence between the typical wing section and the three-dimensional wing can be formulated as follows

$$\begin{bmatrix} \Omega_{tws,1}(P_{tws}) \\ \Omega_{tws,2}(P_{tws}) \\ \mu_{tws,1}(P_{tws}) \\ \mu_{tws,2}(P_{tws}) \\ h^{le}_{tws,1}(P_{tws}) \\ h^{le}_{tws,2}(P_{tws}) \end{bmatrix} = \begin{bmatrix} 2\pi \times 4.76 rad/s \\ 2\pi \times 7.43 rad/s \\ 1.375 \times 10^6 Kg \cdot m^2 \\ 2.523 Kg \cdot m^2 \\ 25.61 m \\ 1.017 m \end{bmatrix} \tag{3.9}$$

Where Ω denotes a frequency, the subscripts 1 and 2 refer to the bending and torsion modes, respectively, μ denotes a modal mass, the superscript le designates the leading edge, $h^{le} = h + (x^{le} - x_c)(\theta = 1)$ is the vertical displacement at the leading edge of the typical wing section and all components of the right hand-side of Equation (3.9) are obtained from the detailed finite element model of the three-dimensional wing. Note that the fact that $h^{le}_{tws,1} \ll h^{le}_{tws,2}$ suggests that despite the bending/torsion coupling, the first mode of the wing is dominated by bending, while the second one is dominated by torsion.

The constraints (3.9) lead to a nonlinear system of equations with six unknowns, which is solved by the Nelder-Mead simplex method (function fminf in Matlab) to obtain

$$m = 2.05 \times 10^3 Kg$$

$$I_\theta = 2.53 \times 10^3 Kg \cdot m^2$$

$$x_G = 1.126m \quad \text{(upstream of section at 68\%)}$$

$$(x_G - x_C) = 0.0642m \quad \text{(G behind C)}$$

$$K_h = 2.046 \times 10^6 N/m$$

$$K_\theta = 5.468 \times 10^6 N/m$$

Using the above numbers, the modified torsional stiffness (see Equation (3.6)) for an acceleration as high as 0.05 Mach/second is $K^{\bullet}_{\Theta} = 5.471 \times 10^6$ Nm. Hence, as expected, $K^{\bullet}_{\Theta} \cong K_{\Theta}$, which supports the conclusion made above regarding the negligible effect of level flight acceleration on the aeroelastic parameters of a system.

4.0 System Identification using ERA

Depending on several factors, among which is the flow regime, an aeroelastic system can behave linearly or non-linearly. This raises a first albeit minor concern as to the applicability of conventional signal processing techniques to the identification of the aeroelastic parameters of an aircraft, or a typical wing section particularly in the transonic regime. Furthermore, an accelerated aeroelastic system is also a time-varying system. This is essentially because the mass, damping and stiffness properties of the "wet" structure are influenced by the free stream velocity V_∞ of this structure, and V_∞ varies with time during an accelerated flight. This raises a second concern as to the continuous parametric identification of an accelerating aircraft using existing signal processing analysis which, in theory, are limited to time independent systems. Both concerns can be addressed by the windowing approach described below, which is in principle applicable to several identification methods.

First note that:

- some methods are capable of identifying the frequency and damping coefficient of the lowest mode of a structure using as few as 2 cycles of the response of this structure to an input perturbation

- for a mode at 10 Hz, 2 cycles corresponds to a time interval of 0.2 second.

- at an altitude of 10,000 ft a level flight acceleration of 0.05 Mach/second corresponds to a horizontal acceleration of 1.6 g's. Such acceleration is beyond the reach of most if not all aircraft.

• during a time-interval of 0.2 second, the speed of an aircraft accelerating at 0.05 Mach/second varies by 0.01 Mach.

• a 1% variation of a Mach number M_∞ has a negligible effect on the frequency and damping coefficient of a wet structure cruising at M_∞.

From the above observations it can be concluded that within a time-window of the order of 0.2 second, an aeroelastic system with a first wet mode at 10 Hz can be considered, for all practical purposes, as a time-invariant system. Furthermore, within a window of that size the aeroelastic response of such a system can be assumed to be linear, as long as the structure itself behaves linearly, which is usually the case for an aircraft excited by an input to a control surface. Hence it can also be concluded, at least in principle, that it should be possible to expand the flutter envelope of an aircraft using its continuous vibration response to input perturbations during an accelerated flight by applying the following simple procedure

1) locate the time instances at which the Mach numbers of interest are reached by the aircraft.

2) for each Mach number of interest, define a time-window of width equal approximately to 0.2 second or two cycles of the expected lowest frequency.

3) within each time-window, apply a suitable signal processing method to identify the frequency and damping coefficient of the wet structure and associate these with the Mach number for which this window is defined.

The window-based identification approach summarized above can be performed either real-time or off-line as a post-processing signal analysis tool. In this work, the Eigenvalue Realization Algorithm (ERA) [3] is chosen to perform the parameter identification.

The ERA is an identification method for linear time-invariant systems. It implicitly assumes that the dynamic response of the given system is sampled at a constant rate. It can handle multi-degree of freedom systems, and is less sensitive to noise than the logarithmic decay method. In order to keep this chapter self-contained, an overview of ERA will be presented along with its fast implementation FastERA [4,5] which is suitable for real-time processing.

4.1 Overview of ERA

In a linear context, damped structural vibrations are governed by the following equations of dynamic equilibrium.

$$M\ddot{q} + D\dot{q} + Kq = f(t) \qquad (4.1)$$

where M, D, K are respectively the mass, damping, and stiffness matrices, and where $f(t)$ denotes the vector of external forces. The above equations can be re-written in state-space form as follows.

$$\dot{x} = kx + Bf(t) \qquad (4.2)$$

$$q = Cx \qquad (4.3)$$

where

(4.4)

$$x = \begin{bmatrix} q \\ \dot{q} \end{bmatrix} \qquad K = \begin{bmatrix} 0 & I \\ -M^{-1}K & -M^{-1}D \end{bmatrix} \qquad B = \begin{bmatrix} 0 \\ M^{-1} \end{bmatrix} \qquad C = \begin{bmatrix} I & 0 \end{bmatrix}$$

Assuming that initially the structural system is at rest, and that it is excited at $t = 0$ by an impulse load $f(t) = u_0\delta(t)$ where $\delta(t)$ denotes the Dirac delta function, the solution of Equations (4.2) and (4.3) is:

$$q(t) = Ce^{Kt}Bu_0 \qquad (4.5)$$

Note that Equation (4.5) is also the solution of Equations (4.2) and (4.3) for $f(t) = 0$ and an initial velocity equal to $M^{-1}u_0$.

For an arbitrary excitation, $f(t)$ can be represented by a series of impulses at discrete time-stations t_i – that is $f(t) = \sum_{i=1}^{\infty} u_i\delta(t - t_i)$, in which case the solution of Equations (4.2) and (4.3) at time t_k is given by

$$q_k = q(t_k) = \sum_{i=0}^{k} Ce^{(t_k - t_i)K}Bu_i = \sum_{i=0}^{k} Ce^{(k-i)\Delta tK}Bu_i \qquad (4.6)$$

where a constant sampling rate $1/\Delta t$ is assumed so that $t_k - t_i = (k - i)\Delta t$.

Let

$$A = e^{\Delta tK} \qquad (4.7)$$

Using the above definition of the matrix A, Equation (4.6) can be re-written as follows.

(4.8)

$$q_k = \sum_{i=0}^{k} CA^{k-i}Bu_i = \sum_{i=0}^{k-1} CA^{k-i-1}(AB)u_i + CBu_k = \sum_{i=0}^{k-1} (CA^{k-i-1}\mathbf{B}u_i) + \mathbf{G}u_k$$

where

$$\mathbf{G} = CB \quad \text{and} \quad \mathbf{B} = AB \qquad (4.9)$$

Hence q_k is the classical solution of the state-space realization problem for the following linear sampled data system.

$$x_{k+1} = Ax_k + \mathbf{B}u_k \qquad (4.10)$$

$$q_k = Cx_k + \mathbf{G}u_k \qquad (4.11)$$

If n_{dof} denotes the total number of degrees of freedom of the computational model described by equation (4.1), but only $n_{dof}^{mes} < n_{dof}$ degrees of freedom are measured, then the matrix C can be written as:

$$C = \begin{bmatrix} L & 0 \end{bmatrix} \qquad (4.12)$$

where L is an $n_{dof}^{mes} \times n_{dof}$ Boolean matrix. Hence, in general, the number of state-space variables x_k that are considered is $n_x = 2n_{dof}$, and the matrix A defined in Equation (4.7) is an $n_x \times n_x$ matrix. In general, the discrete convolution sum (4.8) is expressed as:

$$q_k = \sum_{i=0}^{k} M_{k-1} u_i \qquad (4.13)$$

where the matrices

$$M_k = \begin{cases} \mathbf{G} & , m = 0 \\ CA^{m-1}\mathbf{B} & , m > 0 \end{cases} \qquad (4.14)$$

are known as the Markov parameters. Hence, q_k can be directly related to the load components u_i via the Markov parameters M_i.

Let z_s and $\lambda_s = \alpha_s \pm i\omega_s$ denote the complex eigenmodes and eigenfrequencies of the structure defined by

$$\lambda_s^2 M z_s + \lambda_s D z_s + K z_s = 0 \qquad (4.15)$$

From Equation (4.4), it follows that the λ_s are also the eigenvalues of K, and the eigenvectors of this matrix are

$$y_s = \begin{bmatrix} z_s \\ \lambda_s z_s \end{bmatrix} \qquad (4.16)$$

The ERA exploits the results summarized above as follows. First, it constructs the Markov parameters M_k using the input and output data, namely, the impulse loads and measured displacements. Then, it extracts the matrix A from the Markov parameters M_k using, for example,

the FastERA algorithm described in Section 4.2. Finally, the ERA computes the eigenvalues σ_s and eigenvectors a_s of A which satisfy

$$Aa_s = \sigma_s a_s \qquad (4.17)$$

From Equation (4.7), it follows that the sought-after complex modes z_s, damping ratios ξ_s, and frequencies ω_s of the given structural system are given by

$$z_s = Ca_s \quad \xi_s = \frac{1}{\omega_s \Delta t}\mathrm{Re}\{\ln(\sigma_s)\} \qquad \omega_s = \frac{1}{\Delta t}\mathrm{Im}\{\ln(\sigma_s)\} \qquad (4.18)$$

4.2 The FastERA Algorithm

This work uses the FastERA implementation or the ERA to perform all identifications. For this reason, FastERA is reviewed in this section and some key variables are introduced that appear in the remainder of this work.

The FastERA method is based on the analysis of the following Hankel matrix that is defined for a data set (q_k, u_k) sampled at N points in time

$$H_{qd} = \begin{bmatrix} M_1 & M_2 & \cdots & M_d \\ M_2 & M_3 & \cdots & M_{d+1} \\ \vdots & \vdots & \ddots & \vdots \\ M_q & M_{q+1} & \cdots & M_{q+d+1} \end{bmatrix} \qquad (4.19)$$

and where q and d are such that $N = q + d$. From the definition (4.14) of the Markov parameters, it follows that H_{qd} can be decomposed as follows

$$H_{qd} = V_q W_d \qquad (4.20)$$

where

$$V_q = \begin{bmatrix} C \\ CA \\ \vdots \\ CA^{q-1} \end{bmatrix}, \quad W_d = \begin{bmatrix} B & AB & \cdots & A^{d-1}B \end{bmatrix} \qquad (4.21)$$

The $qn_{dof}^{mes} \times qn_{dof}$ matrix V_q determines the observability of the system whereas W_d is related to its controllability.

The FastERA method starts with the construction of the $qn_{dof}^{mes} \times qn_{dof}$ "square data matrix"

$$J_q = H_{qd} H_{qd}^T = V_q W_d W_d^T V_q^T \qquad (4.22)$$

For a given set of inputs u_k and outputs q_k, the choice of state-space variables x is not unique. Indeed, the input/output relation is not affected by the change of variable $x = T\tilde{x}$, which transforms the realization system, (4.10) and (4.11) into

$$\begin{cases} \tilde{x}_{k+1} = T^{-1} A T \tilde{x}_k + T^1 \mathbf{B} u_k \\ q_k = C T \tilde{x}_k + \mathbf{G} u_k \end{cases} \qquad (4.23)$$

The controllability factors associated with $\tilde{x}$ are

$$\tilde{W}_d \tilde{W}_d^T = T^{-1} W_d W_d^T T^{-T} \qquad (4.24)$$

In particular, choosing $T = (W_d W_d^T)^{1/2}$ leads to $\tilde{W}_d \tilde{W}_d^T = I$. Hence, without any loss of generality, the FastERA algorithm assumes that the state-space variables are chosen so that Equation (4.22) simplifies to

$$J_q = V_q V_q^T \qquad (4.25)$$

From Equation (4.21), it follows that the first $(q-1)n_{dof}^{mes}$ rows of V_q are given by

$$V_q^{(1)} = \begin{bmatrix} C \\ CA \\ \vdots \\ CA^{q-2} \end{bmatrix} \qquad (4.26)$$

and the last $(q-1)n_{dof}^{mes}$ rows of that matrix are given by

$$V_q^{(2)} = \begin{bmatrix} CA \\ CA^2 \\ \vdots \\ CA^{q-1} \end{bmatrix} = V_q^{(1)} A \qquad (4.27)$$

In general, the number of degrees of freedom, n_{dof} associated with a system to be identified is unknown a priori. Indeed, n_{dof} is infinite for any continuous system. In practice the target values for n_{dof}^{mes} and the corresponding number of state-space variables $n_x = 2n_{dof}$ are dictated by the complexity of the model to be realized. Once the user sets these values, the FastERA algorithm computes the n_x largest eigenvalues κ_j of J_q and their corresponding eigenvectors P_j in order to build the square root factorization

$$\tilde{J}_q = P diag(\kappa_j) P^T = (P diag(\kappa_j^{1/2})(diag(\kappa_j^{1/2}) P^T) = \tilde{V}_q \tilde{V}_q^T \tag{4.28}$$

where $P = \begin{bmatrix} p_1 & \cdots & p_j & \cdots \end{bmatrix}$ and $\tilde{V}_q = P diag(\kappa_j^{1/2})$. From Eqs. (4.27) applied to $\tilde{V}$, it follows that

$$A = \begin{pmatrix} \tilde{V}_q^{(1)} \end{pmatrix}^+ \tilde{V}_q^{(2)} \tag{4.29}$$

where $\begin{pmatrix} \tilde{V}_q^{(1)} \end{pmatrix}^+$ is the pseudo-inverse of $\begin{pmatrix} \tilde{V}_q^{(1)} \end{pmatrix}$.

Hence, the extraction of the n_x largest eigenpairs of the $qn_{dof}^{mes} \times qn_{dof}^{mes}$ data matrix J_q is the most computationally significant step of the FastERA algorithm. Keeping q relatively small, say $q \approx d/5$ allows FastERA to operate in real time. For further details on this identification method, refer to [4].

Next, the window-by-window application of the ERA is validated for the identification of the parameters of an accelerating aircraft by a series of numerical simulations designed for an F-16 fighter configuration for which flight test data are available.

4.3 ERA Sample Rate Effects

It is not only expensive to telemeter large amounts of data to the control room, but with multiple programs competing for available bandwidth, and the decrease in available band width due to frequencies being sold for commercial applications, sometimes it is not even possible. Because of the need to minimize the amount of data that must be telemetered to the control room a study was conducted to determine the effects and limitations of reducing the sample rate. Fig. 4.1 shows the effect that various sample rates have on ERA's ability to accurately identify the frequency of the torsional bending modes. This figure shows that for sample rates below about 20 samples per cycle the algorithm cannot accurately identify the damping ratio. For the frequency (see Fig. (4.1)) the algorithm cannot accurately identify below about 8 samples per cycle.

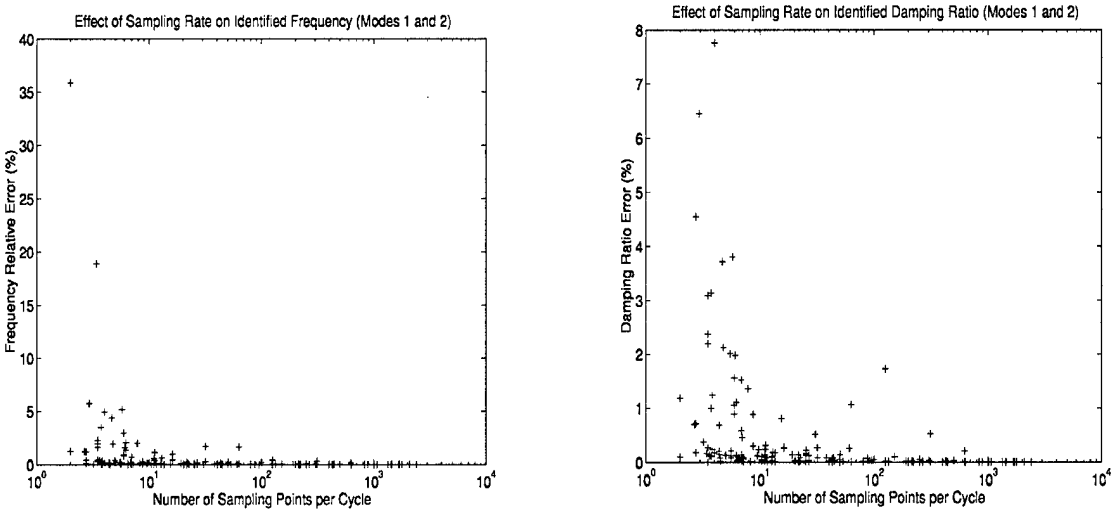

Figure 4.1: Effects of sampling rate on parameters from noise free data

This implies that for clean data (data with no noise) the minimum acceptable sample rate for a ten hertz mode would be about 200 cycles per second. This is marginally within the range of sample rates normally used structural envelope expansion flight testing. However, this is for clean data, and may not work for data with noise.

4.4 ERA Noise Tolerance Study

Realizing that the ERA algorithm is based on Fast Fourier Transforms and all the problems with using small block sizes apply, namely frequency resolution and noise tolerance, a noise tolerance study was conducted in order determine the usefulness of ERA for determining frequency and damping characteristics of noise ridden data.

Noise was generated for this study using the random function in Matlab. The random function produces data that have a level, but not constant frequency content. Noise levels of 1% and 5% were used. The 1% noise level means the highest possible value of the random function is set to 1% of the highest excitation level in the signal. 5% noise is defined in same fashion.

The diagram in Fig. (4.2) shows the scatter of frequency and damping verses the number of samples per cycle. For the damping ratio, the scatter stabilizes at about ½% error at about 1,000 samples per cycle. For the frequency, the scatter stabilizes at about ¾% scatter, and that again is at about the 1,000 sample per cycle. This level of uncertainty might be acceptable, however the sample rate would have to be 5000 samples per second. It is possible, but not practical, to sample and telemeter flight test data real time at that sample rate.

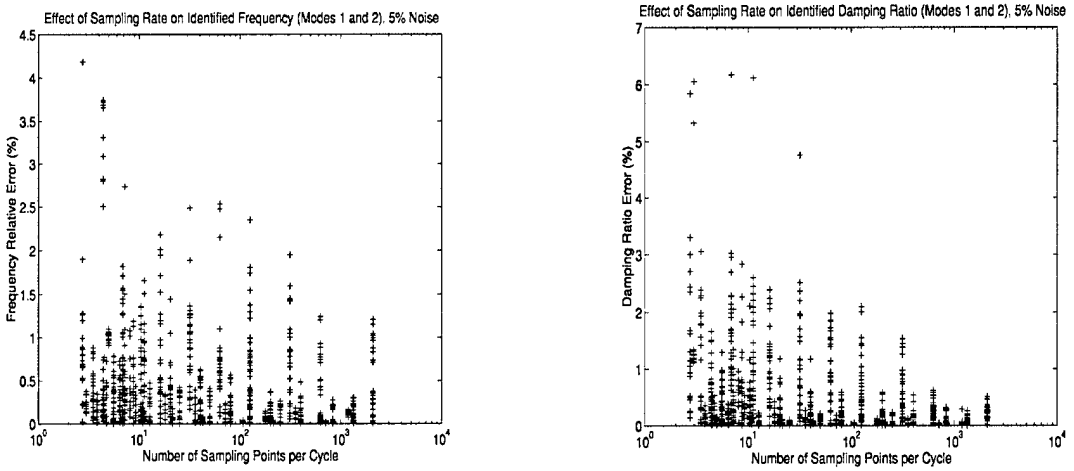

Figure 4.2: Effects of sample rate on parameters from data with 5% noise

4.5 ERA Window Size/Acceleration Rate Study

As a result of this inability to satisfactorily identify modes with a window of 0.2 seconds and noisy data, it was determined that the window size should be increased. But the block size is limited by the acceleration rate. If the Mach number changes too much in the window then the algorithm will fail. So the above noise analysis was conducted with a block size of 1.0 second and the acceleration rate was reduced to 0.01 Mach per second.

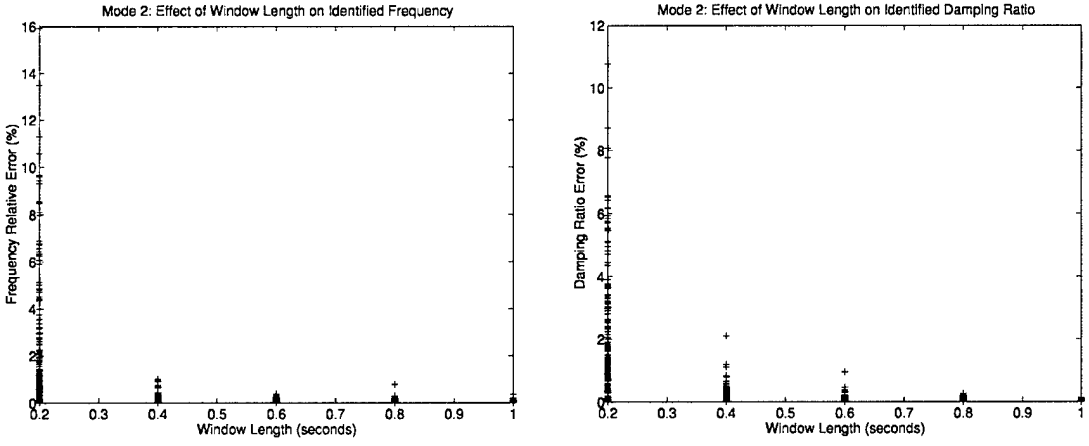

Figure 4.3: Effects of acceleration rate and window size on parameters from data with 5% noise

The results shown in Fig. 4.3 indicate the one-second block is sufficient to identify the parameters even in the presence of 5% noise.

4.6 Validation

There are two things that need to be validated here. They are the two issues that have been examined thus far in this thesis. First, that acceleration does not significantly affect the aeroelastic parameters. Second that the windowing is an effective way to identify the aeroelastic parameters. Both of these validations can be accomplished simultaneously by comparing simulation data from stabilized conditions to simulation data from accelerated conditions. Some critics might not be satisfied with this approach because of the potential that both simulations are flawed. In order to address this concern the data from the simulations will be compared to flight test data provided by the Air Force Flight Test Center. Section 4.6.1 will outline the details of the modeling process for the simulations presented in this chapter, and the simulation technology that is used throughout this document. Details pertaining to how the simulated structure was excited, and how exploiting the moving mesh algorithm enforced the acceleration of the model will also be discussed.

There are minor differences in configuration between the simulations, which represent a clean wing (i.e. no external stores) configuration, and the flight test data which are for a configuration with minimal stores. Also the simulation is a two-dimensional representation of the full three-dimensional aircraft. Even so, the correlation between them is remarkable. Figure 4.6 shows that predicted wet frequencies are in good agreement with those measured in flight test. The predicted damping ratios do not agree as well with the experimental data, even though the trend of their variation with the Mach number is similar to that of the flight test data. As a flutter flight test engineer these results are quite exciting because a simple model is providing better prediction than are typically available to support the flight test.

4.6.1 Simulation Technology

Because the validation is dependent on simulation, it is expedient to explain the technology that was used to perform those simulations. Because these are aeroelastic simulations it is implied that there is some representation of the structure and some representation of the aerodynamics (i.e. the fluid). And the technology would not be complete without discussing the three-field approach that is used to manage the information as it is passed between the structure and the fluid software modules.

4.6.1.1 Structure Model Used for the Simulations

The structure that was used in these simulations is the typical (2 degree of freedom) wing model representation of the F-16 that was developed in chapter 3. For the sake of brevity this model will not be revisited here.

4.6.1.2 Fluid Model Used for the Simulations

The airfoil of the typical wing section was chosen as that of the cross section located at 45% of the distance between the root and tip of the three-dimensional wing because:

- The chord of the airfoil of the typical wing section must be close to the ratio of the wetted area and the wingspan.

- Because the wing is tapered, most of the lift is generated by the section of the wing that is close to the root, which means that the aerodynamic center of the wing is within that area.

The flow domain was discretized by 18,000 vertices, to ensure a sufficient resolution for shock capturing in the region close to the sharp leading edge (Fig. 4.4). Because the purpose of the typical section is to represent the entire wing, each aerodynamic force obtained from a flow computation on this two-dimensional mesh was multiplied by the span of the wing.

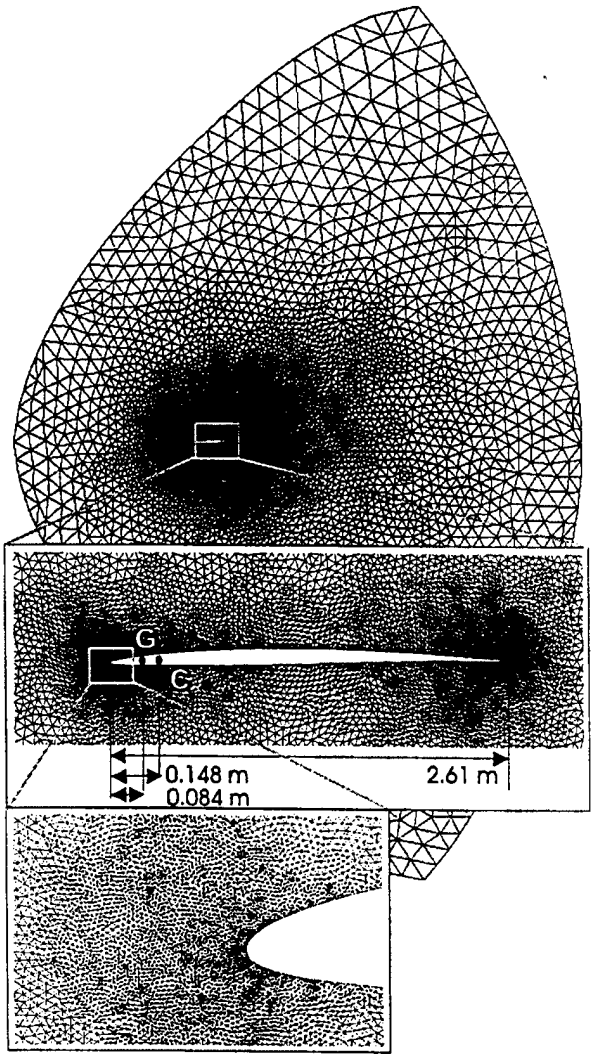

Figure 4.4: Discretization of the flow computational domain (F-16 airfoil)

4.1.6.3 Discrete Fluid Equations of Motion

To adequately describe the motion of the typical wing section, introduced above, requires evaluating the resulting aerodynamic force and moment Q_h and Q_θ. The fluid was modeled using the Arbitrary Lagrangian Eulerian (ALE) form of the Euler equations in order to handle the vibrations of the airfoil and its acceleration.

Let $\Omega(t) = \mathbb{R}^2$ be the flow domain surrounding the airfoil of the typical wing section, and $\Gamma(t)$ be its moving boundary. A mapping function is introduced between $\Omega(t)$ where time is denoted by t and a grid point's coordinates by x, and a reference configuration $\Omega(t)$ where time is denoted by τ and the grid point's coordinates by ξ, as follows.

$$x = x(\xi, \tau); t = \tau \qquad (4.30)$$

The ALE conservative form of the Navier-Stokes equations describing viscous flows on dynamic meshes can be written as

$$\left.\frac{\partial(J\mathcal{W})}{\partial t}\right|_{\xi} + J\nabla_x \mathcal{F}^c(\mathcal{W}, \dot{x}) = 0 \qquad (4.31)$$

$$\mathcal{F}^c(\mathcal{W}, \dot{x}) = \mathcal{F}(\mathcal{W}) - \dot{x}\mathcal{W} \qquad (4.32)$$

Where a dot superscript designates a time derivative, $J = \det(dx/d\xi)$, $\dot{x} = \left.\frac{\partial x}{\partial \tau}\right|_{\xi}$ is the velocity of the dynamic fluid mesh, $\mathcal{W}$ is the fluid state vector (state variables), and $\mathcal{F}^c$ denotes the ALE convective fluxes.

Semi-discretized Equation (4.31) is semi-discretized on a triangulation from which a dual mesh is derived, defined by time-dependent control volumes or cells $C_i(t)$. Resolving the ALE convective fluxes by a suitable Riemann solver. The resulting semi-discrete equation of equilibrium of the fluid is

$$\frac{d}{dt}(A_i W_i) + F_i(W, X, \dot{X}) = 0 \qquad (4.33)$$

Where $A_i = \int_{C_i(t)} d_x\Omega$, W_i denotes the average value of $\mathcal{W}$ over the cell $C_i(t)$, F_i denotes the semi-discrete ALE convective flux, W is the vector formed by the collection of W_i, and X is the vector of time-dependent grid point positions. Various expressions of the flux approximation $F_i(W, X, \dot{X})$ can be found in [6-9]

Time integrate the semi-discrete equations of flow motion (4.33) on dynamic meshes using the generalized second-order implicit backward difference scheme developed in [10,11]. This scheme satisfies the second-order discrete geometric conservation law, and retains second order time-accuracy on moving grids [10,11]. It can be written in compact form as follows.

$$\alpha_{n+1} A_i^{n+1} W_i^{n+1} + \alpha_n A_i^n W_i^n + \alpha_{n-1} A_i^{n-1} W_i^{n-1} + \Delta t^n F_i(W^{n+1}, X_{ave}^{n+1}, \dot{X}) = 0 \qquad (4.34)$$

Where $A_i^n = A_i(X^n)$, and X_{ave}^{n+1}, and $\dot{X}_{ave}^{n+1}$ are the following averaged position and velocity of the fluid moving mesh.

$$X_{ave}^{n+1} = \alpha_{n+1}\left(\frac{X^n + X^{n+1}}{2}\right) - \frac{\alpha_{n-1}}{\zeta}\left(\frac{X^{n-1} + X^n}{2}\right) \qquad (4.35)$$

α_{n-1}, α_n, and α_{n+1} are time dependent because a variable time step $\Delta t(n)$ is employed and are given by

$$\zeta = \frac{\Delta t^n}{\Delta t^{n-1}} \qquad (4.36)$$

$$\alpha_{n-1} = \frac{\zeta^2}{1+\zeta} \leq \qquad (4.37)$$

$$\alpha_n = -1-\zeta \qquad (4.38)$$

$$\alpha_{n-1} = \frac{1+2\zeta}{1+\zeta} \qquad (4.39)$$

It remains to specify how X^n, the vector position of the fluid grid points, is updated at each time-station t^n.

For this purpose, first note that for a typical wing section problem, the simplest strategy for updating the position of the fluid mesh is to move it rigidly with the airfoil. Then note that the motion of the airfoil is completely determined by the motion of the fuselage point F, and the vibrations of the bending and torsional degrees of freedom, h and θ. It follows that at each time-station t^n, the position of any fluid grid point N is given by:

$$x_N^n = x_F^n + (x_N^0 - x_F^0)\cos\theta^n - (y_N^0 - y_F^0)\sin\theta^n \qquad (4.40)$$

$$y_N^n = y_F^n + h^n + (y_N^0 - y_F^0)\cos\theta^n - (x_N^0 - x_F^0)\sin\theta^n \qquad (4.41)$$

Where h^n and θ^n are determined by solving the coupled fluid/structure equations of motion (3.3), (3.4), and (4.33), and the instantaneous position (x_F^n, y_F^n) of the fuselage point F is deduced from the specified acceleration of the aircraft. For example, for a constant acceleration, the instantaneous position of the point F is given by:

$$x_F^n = \frac{\gamma_{F_x}}{2} t^{n^2} + x_F^0 \qquad (4.42)$$

$$y_F^n = \frac{\gamma_{F_y}}{2} t^{n^2} + y_F^0 \qquad (4.43)$$

Hence, the acceleration of the typical wing section is transmitted to the fluid by Equations (4.42), and (4.43), and accounted for by the additional convection term $\dot{x}\mathcal{W}$ that characterizes the ALE form (4.31) of the flow equations.

Remark. At the first glance, the reader may think that Equations (4.42), and (4.43) are missing the terms $V_{\infty_x} t^n$ and $V_{\infty_y} t^n$ where V_∞ is the free-stream velocity. However, these terms are not missing. They are automatically taken into account by the initial conditions of the CFD simulation through the specified free-stream Mach number M_∞.

The coupled fluid/structure discrete equations of motion are solved, throughout this chapter, by the second-order time-accurate staggered and sub-iteration free algorithm described in [12]. As stated earlier, this staggered algorithm is equipped with the midpoint rule as a structural time-integrator, and

the generalized second-order implicit backward difference scheme (4.34) developed in [10,11] as a flow time-integrator

4.6.1.4 The Three Field Approach

In order to combine the computational fluid dynamics, which utilizes a coordinate system, fixed in space (Eulerian coordinate system), and the finite element method, which utilizes a coordinate system, fixed to the material (Lagrangian coordinate system), it is critical to allow the computational fluid dynamic mesh to move to accommodate the motion of the finite element mesh. The method used to allow the motion of the fluid mesh is to formulate the mesh as a psudo-structural system. The combination of the computational fluid dynamics, the finite elements, and the psudo-structural fluid mesh system is known as the three field formulation. The way the three field formulation works is through message passing between the three software modules. The finite element module sends displacement information to the mesh motion module which calculates the motion of each grid point in the fluid mesh. The mesh motion is then sent to the computational fluid dynamic module. The computational fluid dynamics module calculates the fluid states for each cell of the fluid grid. The fluid flux related to the motion of the fluid mesh is accounted for using the Arbitrary Lagrangian Eulerian (ALE) formulation described in reference [13]. The pressure is then sent to the finite element module and the cycle is complete. The timing of the message passing is important to maintain the order of accuracy of the simulation. The staggered approach described in reference [14] is used for this reason. The equations governing each algorithm are listed below.

Fluid Equation

$$\left.\frac{\partial(Jw)}{\partial t}\right|_{\xi} + J\nabla\bullet\left(F(w) - \frac{\partial x}{\partial t}w\right) = 0 \qquad (4.44)$$

Structure Equation

$$\rho_s \frac{\partial^2 u_s}{\partial t^2} - div\left(\sigma_s\left(\varepsilon_s(u_s), \frac{\partial \varepsilon_s}{\partial t}(u_s)\right)\right) = b \quad (4.45)$$

Mesh Motion Equation

$$\tilde{\rho}\frac{\partial^2 x}{\partial t^2} - div\left(\tilde{\sigma}\left(\tilde{\varepsilon}(x), \frac{\partial \tilde{\varepsilon}}{\partial t}(x)\right)\right) = 0 \quad (4.46)$$

There are also some boundary conditions that must be observed. First on the boundary between the fluid and the structure the normal pressure of the fluid has to equal the normal stress of the structure and the normal velocity of the fluid has to equal the normal velocity of the structure. Second the normal displacement and the normal velocity of the fluid mesh and structure must be equal along the boundary between them.

Fluid/Structure Interface Conditions

$$-pn = \sigma_s \cdot n \quad (4.47)$$

$$\frac{\partial u_F}{\partial t} \cdot n = \frac{\partial u_s}{\partial t} \cdot n \quad (4.48)$$

Fluid mesh/Structure Interface conditions

$$x = u_s \quad (4.49)$$

$$\frac{\partial x}{\partial t} = \frac{\partial u_s}{\partial t} \quad (4.50)$$

4.6.2 Numerical Aeroelastic Simulations

The altitude was fixed at 3,000 m, the angle of attack was set to 0 degree, and the first of a series of aeroelastic simulations was performed for a sequence of stabilized flight conditions at the following Mach numbers: 0.8, 0.85, 0.875, 0.9, 0.925, 0.95, 1.0, 1.1, 1.2, 1.3, and 1.4. For each Mach number, the numerical simulation starts from a steady-state flow and the following initial conditions for the typical wing section: $\dot{h}^0 = 0.01$ m/s, and $\dot{\theta}^0 = 0.2$ rad/s. Fig. 4.5 and Fig. 4.6 present the predicted transient responses of the structure at $M_\infty = 0.8$, and $M_\infty = 1.0$, respectively. These figures show that at $M_\infty = 0.8$, the aeroelastic vibrations are rapidly damped out. They also show that at $M_\infty = 0.8$, both modes of the typical wing section contribute initially to the bending degree of freedom (θ). It can be concluded that it is the bending mode of the typical wing section that is rapidly damped out at $M_\infty = 0.8$. The history of $\theta(t)$ graphically depicted in Fig. 4.6 reveals that flutter or limit cycle oscillations are initiated at $M_\infty = 1.0$.

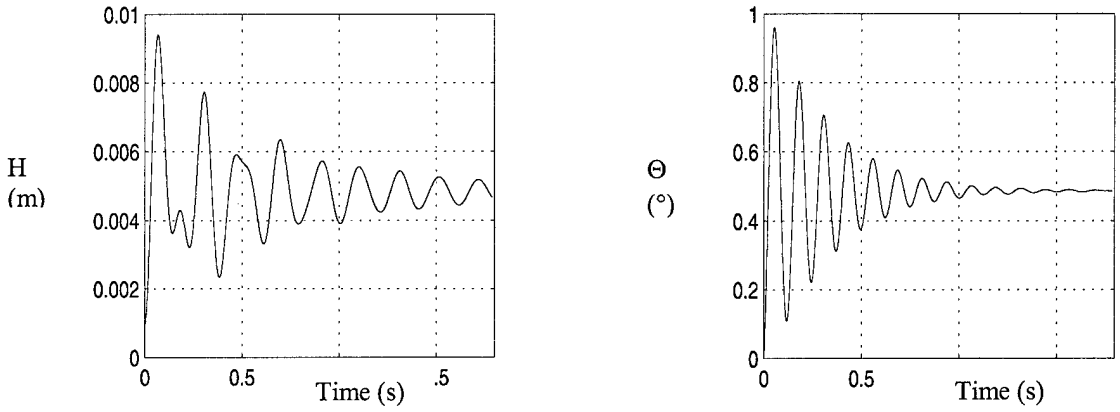

Figure 4.5 Transient aeroelastic response for stabilized flight conditions at Mach = 0.80

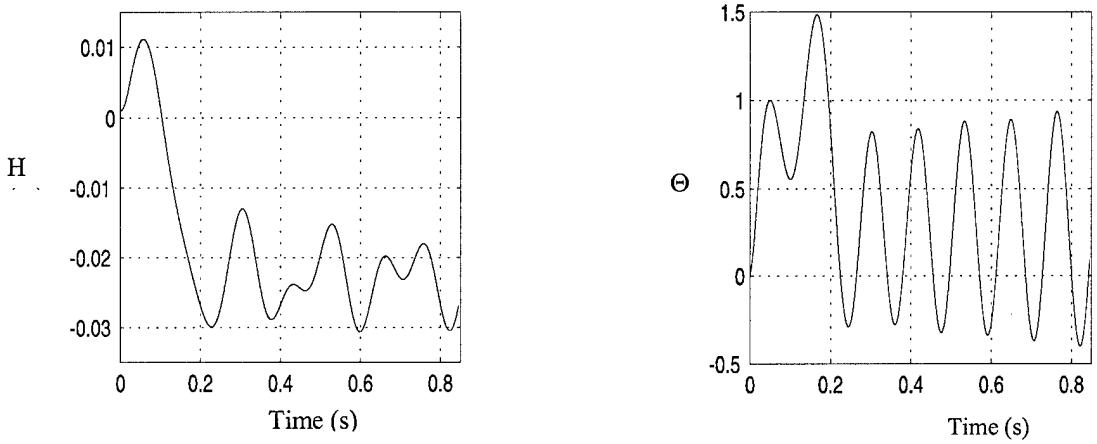

Figure 4.6 Transient aeroelastic response for stabilized flight conditions at Mach = 1.00

Next the aeroelastic response during accelerated flight of the typical wing section is simulated at the rate of 0.05 Mach/second. The reader is reminded that such acceleration is even higher than what an F-16 can achieve in a level flight. This simulation was initiated at $M_\infty = 0.75$ and excite the structure with the same initial conditions as previously: $\dot{h}^0 = 0.01$ m/s, and $\dot{\Theta}^0 = 0.2$ rad/s. It is reported in Fig. 4.7 the predicted response of the structure. The reader can observe that both modes of the typical wing section contribute to the early response of the h degree of freedom. The significant

decrease of the mean value of h that is noted between Mach 0.85 and Mach 0.95, suggests an important drop in the lift in this Mach region, which, given that the F-16 airfoil is unsymmetric. This is indicative of the appearance of a shock and reaching the Mach divergence speed. Most importantly, Fig. 4.7 shows that between Mach 0.85 and Mach 0.95, the vibrations of h and θ become too small to allow a parametric identification. Hence, it can be concluded that a continuous parametric identification of an aircraft that accelerates across the subsonic, transonic, and supersonic regimes requires systematic re-excitations.

In order to illustrate the effect of re-excitation, a second accelerated flight was simulated where the initial speed corresponds to Mach number 0.84, and the initial excitation is effected by the same initial conditions as previously. The computed aeroelastic response is reported in Fig. 4.8. This response is characterized by larger amplitudes of vibration between Mach 0.85 and Mach 0.95, and confirms that flutter or limit cycle oscillations initiate around Mach 1.0.

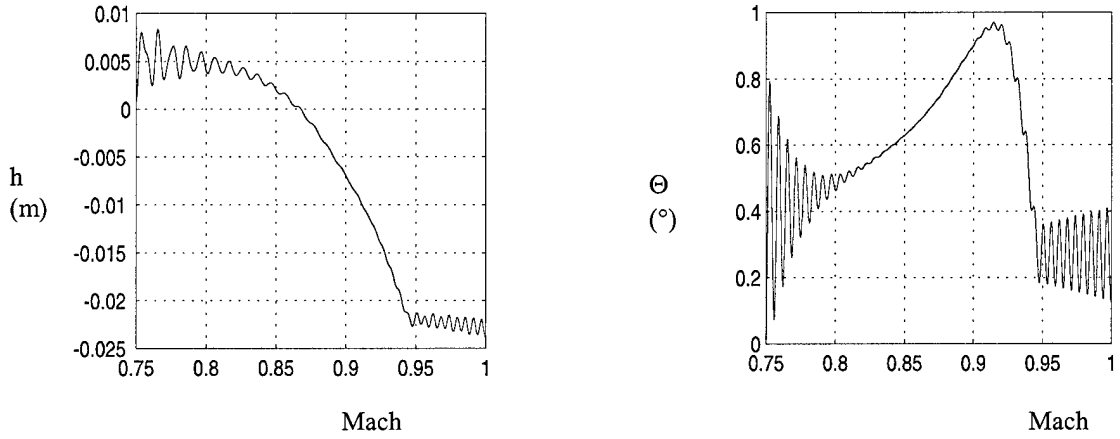

Figure 4.7 Transient response during an accelerated flight: initial speed corresponds to Mach 0.75 and is increased by 0.05 Mach/second

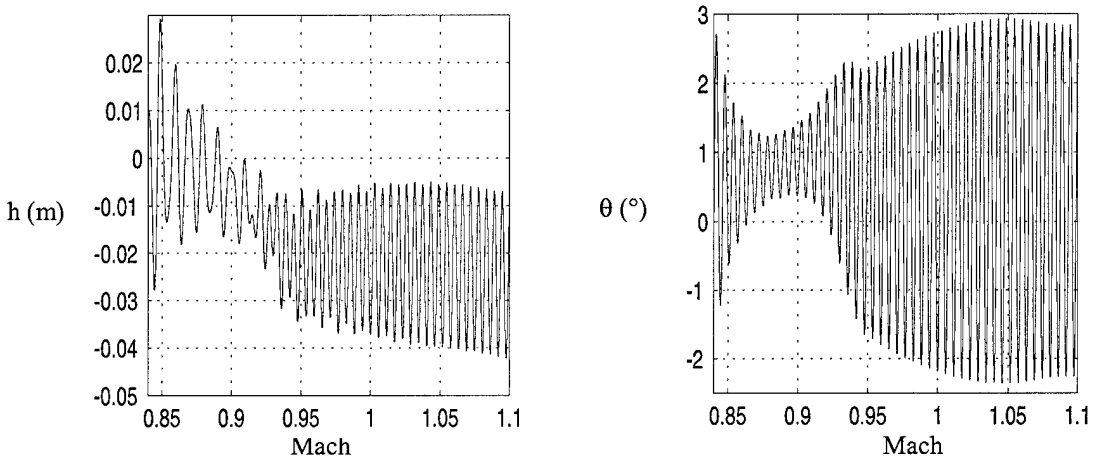

Figure 4.8 presents the simulated aeroelastic response of the accelerated typical wing section after re-excitation at Mach 1.04.

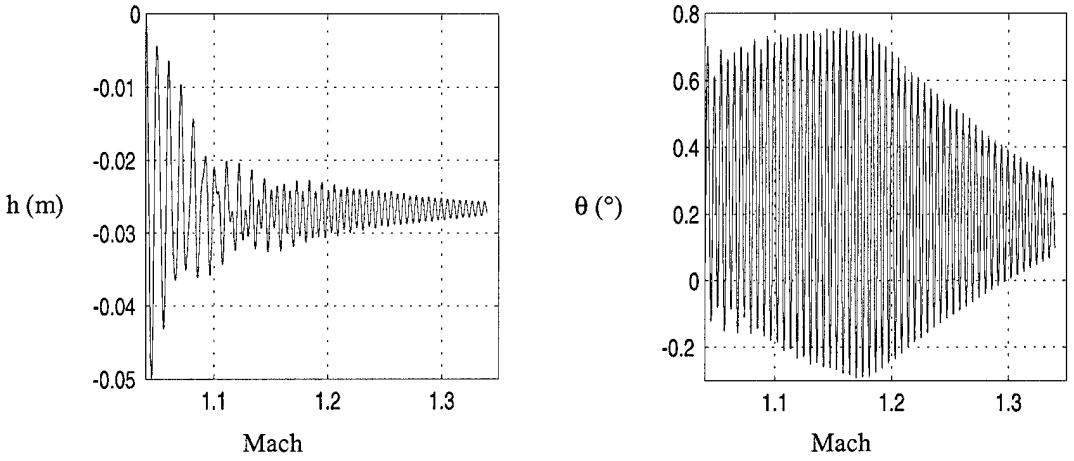

Figure 4.9 Transient response during an accelerated flight: initial speed corresponds to Mach 1.04 and is increased by 0.05 Mach/second

4.6.3 Validation of the 2 Dimensional Simulation

As stated in Section 4.0, the ERA assumes a constant sampling rate. Since the numerical simulations are not performed with a constant time-step Δt, the simulation results are post-processed by using a quadratic interpolation scheme in order to generate signals with a constant sampling rate.

The typical wing section described in this chapter has 2 degrees of freedom. However, the aeroelastic typical wing section has more than 2 degrees of freedom, because of the surrounding fluid. For this reason, in all cases discussed in this section, the number of states for the synthesized system is set to $n_x = 10$, as if the system contained 5 degrees of freedom.

ERA requires two cycles of the lowest mode contributing to the signal, and about 500 sampling points per cycle in order to accurately identify the system. Hence, in this work the parameters of the ERA are set as follows

$$
\begin{aligned}
&1000 \le N \le 6000 \\
&500 \le q \le 1000 \\
&500 \le d \le 5000 \\
&2\frac{T_1}{N} \le \Delta t_s \le 3\frac{T_1}{N} \\
&n_x = 10
\end{aligned}
$$

Where Δt_s is the sampling rate, and T_1 is the period of the lowest frequency mode. It was verified a posteriori that the ERA configured with the above parameters produced excellent results for all applications discussed in this work. Nevertheless, it was noted that higher values of the number of samples N and higher values of q improve the accuracy of the identification, but increase its cost.

As explained in Section 4.0, in order to extract the aeroelastic parameters of the typical wing section from the signals generated by the accelerated flight simulations, ERA with windowing were

employed. The size of each time-window is $N\Delta t$. Given that the frequency of the first wet mode of the system can be expected to be close to that of the first dry mode of the system – that is 4.7 Hz –it follows that the size of each time-window varies between 0.4 second and 0.6 second. Hence, for an acceleration of 0.05 Mach/second, the maximum variation of the Mach number within a time-window is about 0.03 Mach. The significance of this variation depends on how fast the damping coefficient of the structure varies with the Mach number, which depends on the flow regime. Extensive experiments have revealed that when using the ERA with windowing, the identification results are to some extent insensitive to small variations in the size of the time-window and/or the values of n_x, q, and d.

The frequencies and damping ratios identified by the FastERA using stabilized and accelerated flight simulation data are reported in Fig. 4.10 and Fig. 4.11. The following observations are noteworthy

• The typical wing section exhibits flutter for the second (torsional) mode in the transonic regime, for $0.89 \leq M_\infty \leq 1.1$.

• A sharp decrease of the damping ratio ε_2 of the torsional mode occurs around Mach 0.9, and a slow increase of that damping ratio occurs above Mach 0.92. The same trend was also observed for the damping ratio ε_1 of the first mode; however, ε_1 remains positive.

•The frequency of the first mode appears to be almost independent of the Mach number. On the other hand, the frequency for the torsional mode, which is responsible here for flutter, increases slightly with the Mach number.

• Occasionally, the frequencies and damping ratios identified for the first mode in simulated accelerated flight are reported to be different from those identified using stabilized flight simulated data. This is due to the fact that in the accelerated flight simulation, because the system is excited only

at the beginning of the flight segment, after a certain amount of time, the contribution of the first mode to the signal can no longer be identified because it becomes significantly damped out. Re-exciting the system every second or so cures this problem.

• For the second mode, the frequencies and damping ratios identified for the stabilized and accelerated flight scenarios are in good agreement.

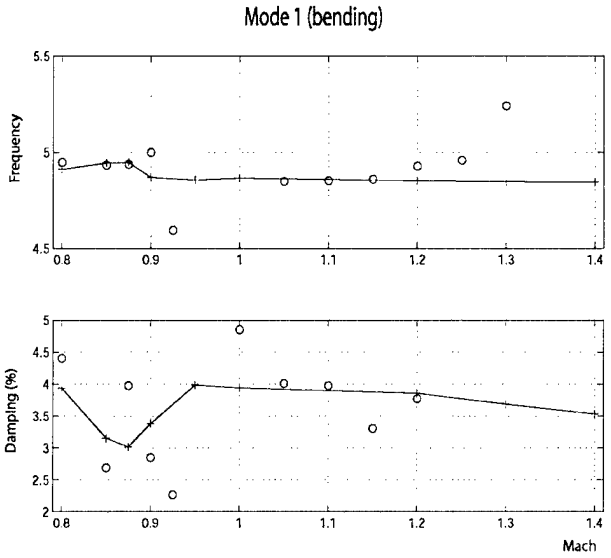

Figure 4.10: Identified first bending (Mode 1) frequencies and damping ratios for stabilized and accelerated simulation data from the typical wing section of an F-16 aircraft.

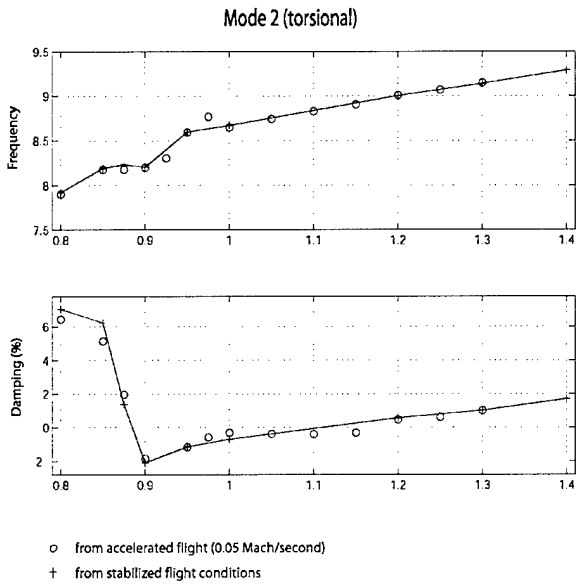

Figure 4.11: Identified first torsion (Mode 2) frequencies and damping ratios for stabilized and accelerated simulation data from the typical wing section of an F-16 aircraft.

So it is reasonable to conclude that for the simulated data the acceleration does not significantly affect the aeroelastic parameters. It can also be concluded that using the windowing approach the aeroelastic parameter could be identified using the accelerating data.

Now the simulated data and the flight test data provided by the Air Force Flight Test Center are compared. The simulation results and test data are for the same stabilized flight conditions, but not exactly the same F-16 configuration. The typical wing section designed in this paper is for a clean-wing configuration of the F-16. The flight test data provided by the Air Force Flight Test Center are for a configuration of the F-16 that includes pylons and missiles. Nevertheless, Fig. 4.11 shows that the predicted wet frequencies are in good agreement with those measured in flight test. However, the predicted damping ratios do not agree well with the experimental data, even though the trend of their variation with the Mach number is similar to that of the flight test data. It can reasonably be argued

that a major cause of this discrepancy is the typical wing section model, which is supposed to be realistic only for fairly homogeneous wings with high aspect ratios and angles of sweep.

It has been shown that ERA can be used with the windowing technique developed to identify modal parameter of an accelerating aeroelastic system. It has also been demonstrated by way of simulation, not only that the modal parameters can be identified from the data of an accelerating system, but the acceleration does not significantly change the modal parameters of the system at any particular Mach number. The results of this validation were so compelling that the Air Force Flight Test Center agreed to conduct a test program during which they flew accelerated and stabilized test points. The details of this test program are the subject of next chapter, and the results will be used in chapter 6 to accomplish further validation of the accelerated flutter test.

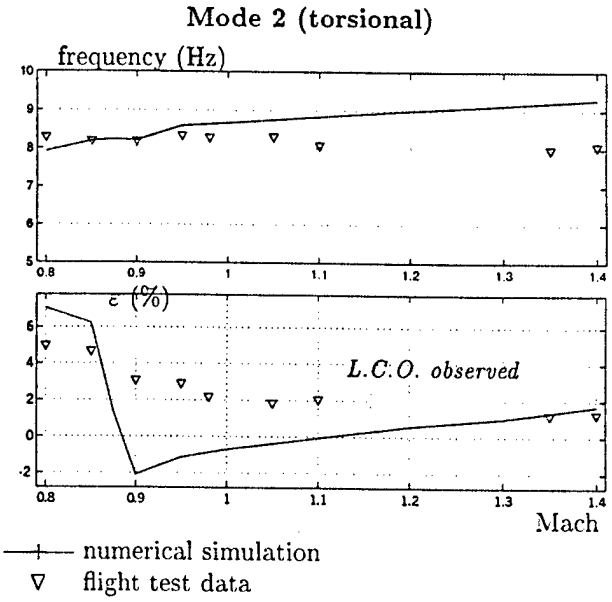

Figure 4.12: Validation of ERA using windowing and Accelerated Flutter Testing using pre-1998 data and two degree of freedom F-16 model

5.0 Flight Test of an F-16 Configuration

Encouraged by the results of the two degree of freedom F-16 typical wing section model the Air Force Flight Test Center wanted to see results for full aircraft simulations, and supported the effort with flight test data flown specifically for this project by the United States Air Force Test Pilots School (TPS). In May of 2000 the TPS flew three sorties in order to collect flight test data for aeroelastic and Limit Cycle Oscillation conditions. It is interesting to note that five sorties were planed, but all the data were collected in two sorties (one sortie was unproductive due to instrumentation problems). One explanation for this unexpected efficiency is the points were being flown using accelerations rather than stabilized test points. The testing was done as a staff project of the TPS. The TPS was designated the Responsible Test Organization (RTO) and the 416 FLTS (F-16 Combine Test Force) was designated the Participating Test Organization (PTO). This project was named "Have Zip".

5.1 Test Item Description

The F-16C aircraft, serial number S/N 87-0352 was the test aircraft used for these tests. The aircraft was equipped with a flutter excitation system (FES). This system has the capability to drive the flaperon servo actuators symmetrically or antisymmetrically. The FES can provide random burst inputs or sinusoidal burst or sweep inputs at flaperon amplitudes up to ±1 degree.

5.2 Overall Test Objective

The test objective for this flight testing was to collect flight test data for the F-16 in a clean wing and a LCO configuration to support the validation of the accelerated flutter flight test technique.

5.3 Test Resources

5.3.1 Test Aircraft Loadings

Testing was performed using 2 loadings as shown in table 5.1. The aircraft was flown in both the clean wing (no external stores) and in a store loading that provided moderate LCO condition. Mass properties information in the vertical and lateral directions were required for all stores used on this program. The following stores were required:

1) Four AIM-120 missiles (AMRAAM)
2) Six LAU-129 launchers
3) One 300 gallon fuel tank (Optional)

Table 5.1

Have Zip Test Loadings

Loading	Station 1	Station 2	Station 3	Station 4	Station 5	Station 6	Station 7	Station 8	Station 9
1					(Opt)				
2					(Opt)				

AIM-120

300 Gallon Tank on 16S951 Universal Centerline Pylon

LAU-129 Pylon

5.4 Test Execution

The purpose of this test program was to acquire actual aircraft accelerometer and strain gage response data. The data are being used to validate the accelerated flutter testing approach.

5.4.1 Test Objectives

Test Objective 1

Collect baseline dynamic response data from an F-16 Block 40 aircraft (without stores) during accelerations to supersonic conditions and during elevated g conditions in which the aircraft flexible modes are being excited regularly.

Measure of Performance (MOP)1

All clean loading test points in Appendix 2 have been performed and are flown within specified tolerances.

Success Criteria

MOP1 was satisfied when all critical data were acquired for each test maneuver.

Test Objective 2

Collect dynamic response data from an F-16 Block 40 aircraft with a store loading yielding LCO during accelerations to supersonic conditions and during elevated g conditions in which the aircraft flexible modes were being excited regularly.

MOP 2

All store loading test points in Appendix 2 were performed and were flown within specified tolerances.

Success Criteria

MOP2 was satisfied when all critical data were acquired for each test maneuver.

5.4.2 Data Requirements

The data for all test points were acquired using Interactive Analysis and Display System (IADS) [27]. The data were then converted to engineering units in an ASCII format using IADS.

5.5 Test Procedures

Flight testing consisted of two flight test loadings. One clean wing and one store loading. The clean wing loading was flown first on 12 May 2000 (flight 705). The store loading was flown on 15 May 2000 (flight 706). After flight 705 it was discovered that the instrumentation was not functioning properly so the clean wing maneuvers were flown again on 16 May 2000 (flight 707). Test maneuvers consisted of straight and level accelerations from 0.6 to 1.2 Mach number and windup turns. All maneuvers began at 10,000 feet Mean Sea Level (MSL). The flutter excitation system (FES) was used in the antisymmetric flaperon random burst mode for each test point in order to excite the aircraft structural modes. The general test procedures were as follows.

1. Set up at 10,000 feet MSL and 0.6 Mach number and perform level accelerations to 1.2 Mach number while activating minumum duration antisymmetric random bursts (at about 1 second intervals) throughout the runs. The excitation amplitudes may be altered in flight depending on in-flight response data. The first level acceleration was performed starting at MIL power (maximum power available without using afterburner) and then throttling to MAX power (Maximum available power using afterburner) at an

acceleration rate of approximately 2-3 knots per second. The second level acceleration will be performed using MAX power from the beginning to the end of the maneuver.

2. Set up 10,000 ft MSL and test Mach Number. Perform a Wind Up Turn (WUT) to a target load factor and initiate an antisymmetric random burst while maintaining load factor. Perform 2 more random bursts allowing response to decay (approximately 3 seconds) before initiating next burst.

5.6 Test Execution

5.6.1 Instrumentation Checkout

Prior to initiating any test maneuvers on each flight. The pilot performed an instrumentation validation check. The instrumentation check was performed at 0.8 Mach number, 10,000 feet MSL. The loads instrumentation validation check consisted of the following maneuvers:

1) 3.5g windup turn (WUT)
2) 1g 180 degree roll in both directions
3) Wings level sideslip (WLSS) in both directions with slow release.

5.6.2 Test Approach

A crew consisting of a pilot test conductor, test engineer were present for each flight. All test points were initiated at 10,000 ft MSL. Test points consisted of level accelerations and WUT's were perfomed at 0.6, 0.75, 0.9, 0.95, 1.05, 1.2 Mach number.

5.6.3 Test Procedures

Prior to setting up at the test condition, the pilot would verify that the appropriate FES selections were current. For the level acceleration test points, and for the WUT's the pilot stabilized at the beginning Mach number for 10 seconds. The test engineer provided clearance to initiate the maneuver through the test conductor. The pilot then performed the maneuver.

For the clean configuration, there was no requirement in the order in which the test points were accomplished. The desired test sequence was as follows:

1) Set up at the test Mach number in trimmed, straight and level flight.
2) With the throttle in military rated power (maximum power available without using the after burner), apply throttle as needed to begin a level acceleration to 1.2 Mach number exercising the FES with 1-2 seconds between bursts.
3) Reduce speed to 0.6 Mach number and stabilize at 10,000 ft MSL, 0.6 Mach number.
4) With the throttle in Max power, begin a level acceleration to 1.2 Mach number exercising the FES with 1-2 seconds between bursts.
5) Reduce speed to 0.6 Mach number and stabilize at 10,000 feet MSL, 0.6 Mach Number
6) Initiate a left WUT and hold at 3g.
7) Run a 2-second antisymmetric random burst three waiting 3 seconds between bursts to allow the aircraft response to dampen.
8) After completion of the random excitation, pause for 3 seconds and increase load factor to 5g.
9) Repeat step 7.

10) Pause for 3 seconds after completion of random excitation, then return aircraft to 1-g level flight at the target Mach Number and altitude.

11) Repeat steps 6-10 for each remaining target Mach number building up in Mach Number.

These steps were the same as were used for the store loading except that the test point sequence must follow the buildup sequence outlined.

5.6.4 Test Maneuvers

5.6.4.1 Level Acceleration

The aircraft was trimmed to a 1-g flight condition. A level acceleration was performed to the end Mach number initiating the acceleration at MIL or MAX thrust as determined by the test point. The maneuver was ended at MAX thrust setting. During the acceleration, 2-second antisymmetric random bursts were performed at the specified burst amplitude with 1-2 seconds between bursts.

5.6.4.2 Wind Up Turn

The aircraft was trimmed to a 1-g flight condition. A stabilized g turn was performed by banking the aircraft into a turn and applying longitudinal stick force to increase load factor at a rate of less than 2g per second to the target load factor. The throttle could be modulated as required to maintain test conditions. The pilot then initiated a single 2-second random burst at

the specified burst amplitude and allowed the aircraft response to dampen for 3 seconds while load factor was mantained. The pilot repeated the bursts until 3 bursts had been performed.

5.6.4.3 Tolerances

The following tolerances were adhered to for all test maneuvers:

Mach number	±0.02
Altitude	±1000 ft
Nz	±0.2g

5.6.5 Post Test Briefing

After each mission a post flight briefing was conducted to discuss aircraft status, instrumentation status, review the test points completed, and plan the next flight.

5.7 Flight Test Results

The frequency and damping plots for the clean wing data that were collected during this test program are presented in Fig 5.1 and 5.2. Figure 5.1 shows the data for the accelerated flight test points. The curve that is designated as "normal" corresponds to the accelerated test point that was flown using military rated power (i.e. maximum available power without using afterburner). The curve that is designated as "maximum" corresponds to the accelerated test point that was flown using afterburner. Two effects that contribute to the discrepancy between the two test points are the vibration environment caused by the afterburner, and the fuel configuration. The afterburner

significantly increases the ambient vibration environment, which raises the noise floor for the data, and reduced the signal-to-noise ratio. The erratic damping measurements are likely due to this effect. Because the test points were performed at different times during the test flight there would be a different fuel load in each case. A change in the fuel load can change the frequency and damping characteristics of the system under test. The change in frequency between the two test points is possibly the result of different fuel loads.

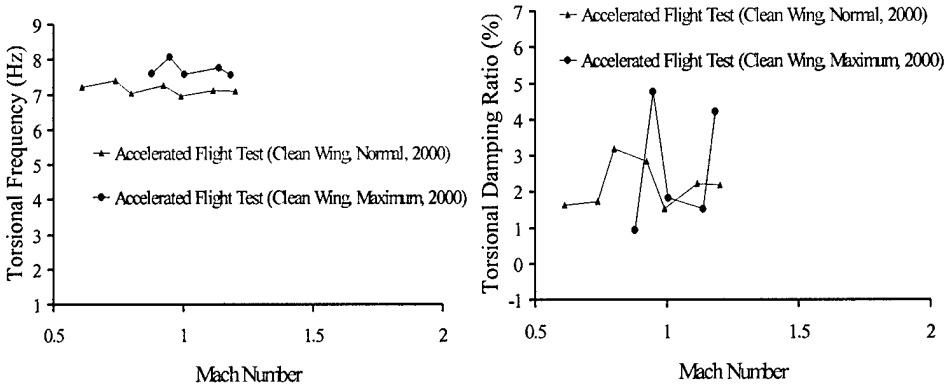

Figure 5.1: Frequency and damping plots for flutter flight tests utilizing stabilized, accelerated normal thrust, and accelerated maximum thrust conditions

Figure 5.2 presents the elevated g maneuvers contrasted against the normal level acceleration. One interesting trend is where the mach dip occurs in each case. As the g factor increases, the angle of attack also has to increase. When the angle of attack increases the flow acceleration over the wing, the unsteady shock wave that causes the Mach dip will occur at a lower Mach number consistent with the flight test data that was collected.

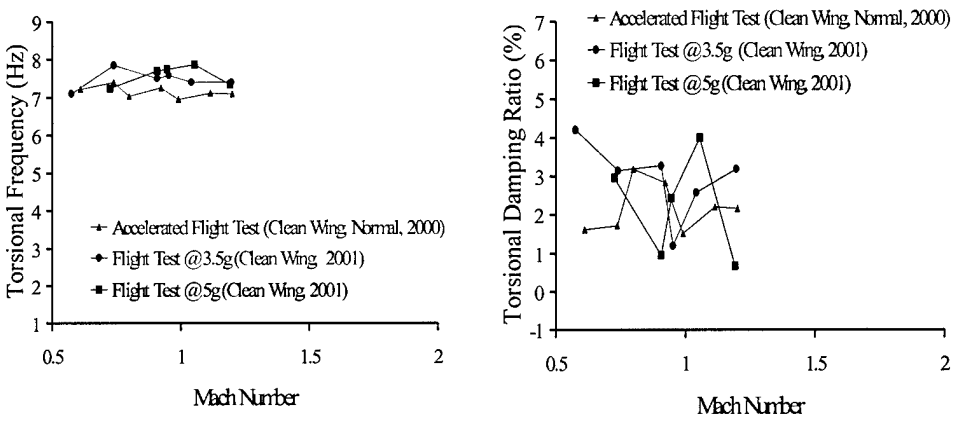

Figure 5.2: frequency and damping data for 1g, 3.5g, and 5g flight test data

This flight test data will be used in chapter 6 in order to validate the accelerated flutter flight test approach.

6.0 3-D Simulation of an F-16 Configuration

In this chapter the concept of accelerated flutter flight test, and that aeroelastic parameters are insensitive to acceleration will be further validated using 3-D simulations. Recall that in chapter 4 the validation using 2-D simulations yielded encouraging results, but still left room for improvement. The flight test data, for an F-16 Block 50 aircraft (shown in Fig 6.1) with no external stores (clean wing) that are described in chapter 5, and full 3-D simulation data of this F-16 configuration will be compared to perform this validation. An additional benefit to validating the accelerated flutter flight test approach using simulations is that the simulation technology will also be validated. The F-16 was selected for these full aircraft simulations because models were obtainable. Lockheed-Martin, Fort Worth with the approval of the F-16 Systems Program Office released two structures models. The Air Force Research Lab, Wright Patterson AFB released the surface geometry that was used to create the fluid grid. These models required many refinements in order to bring them up to the resolution needed for the simulations. Before the validation data are presented, an overview of the structural, and aerodynamic model refinements, and the simulation technology will be presented.

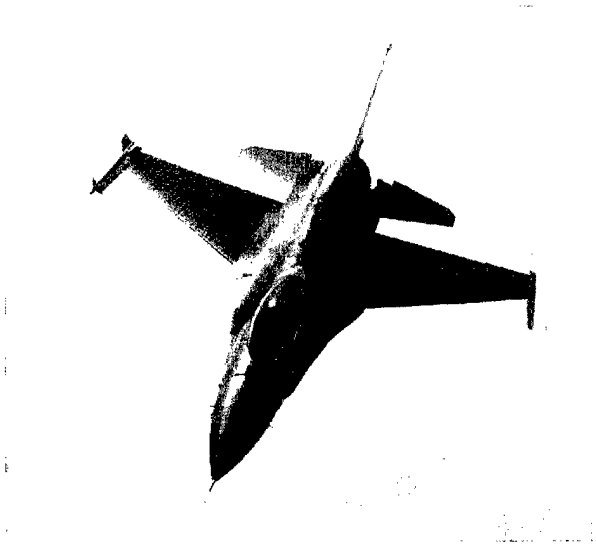

Figure 6.1: Air Force F-16 Block 50 military fighter aircraft

6.1 Structural Model of the F-16

The models that were obtained from Lockheed-Martin were a structural dynamic model (shown in figure 6.2), and a higher fidelity static loads model (shown in figure 6.3).

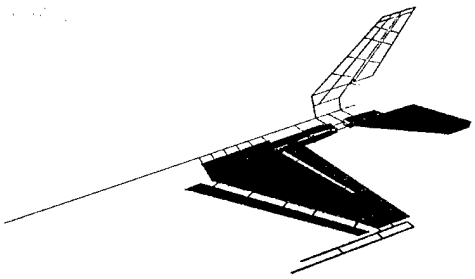

Figure 6.2: F-16 Block 50 structural dynamic model Provided by Lockheed-Martin.

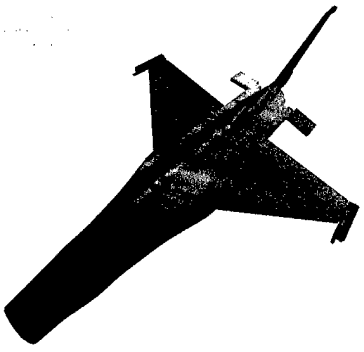

Figure 6.3: F-16 Block 50 static loads model provided by Lockheed-Martin.

Due to the computational resources that were available when these models were created, the resolution of the structural dynamics only has about 1000 degrees of freedom. Because this model is so coarse it was necessary to merge the mass data with the static loads model. In addition to the addition of mass to the static loads model there were a number of refinements required so it would match the aerodynamic model. These refinements were needed so that the structural model would match the aerodynamic model. It is necessary for the structural model to match the aerodynamic model so that the software can determine where on the structure to apply the aerodynamic (pressure) loads. The following figures show in detail the refinements that were made in order to achieve this matching. Figure 6.4 shows the nosecone and part of the canopy missing in the original static loads model. These were not modeled originally because they are not structural members. However they were needed for the aeroelastic simulations. Figure 6.5 shows the final composite structural dynamics model with phantom elements representing the nosecone and canopy. Figure 6.6 shows the horizontal stabilizer of the original static loads model and the overlaid surface geometry. Notice the horizontal stabilizers look like rectangular blocks, and they don't match the anhedral angle of the actual geometry. Originally there was no need to match the geometry exactly, but for the aeroelastic simulations it will be necessary so that the aerodynamic pressure loads could be properly applied to the structural surface. Figure 6.7 shows the gap between the control surfaces and the wing. This gap was bridged using phantom elements. Figure 6.9 show the final composite structural dynamics model without the gap. This was an extensive effort that took approximately 9 man months.

Figure 6.4: Nosecone and aft canopy missing on Original static loads model

Figure 6.5: Phantom elements represent nosecone on final model

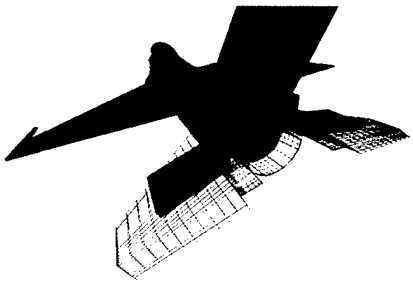

Figure 6.6: Horizontal stabilizers do not Match the surface geometry of the aircraft

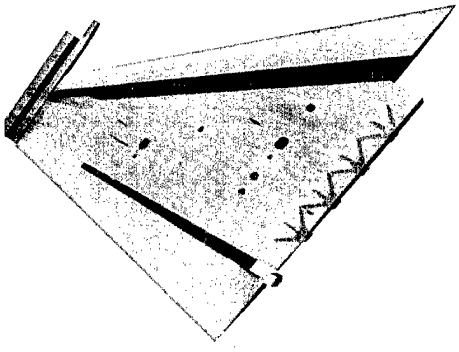

Figure 6.7: Gaps between wing and control surfaces on original static loads model

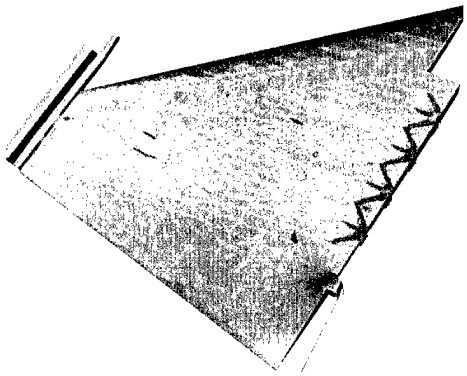

Figure 6.8: Gaps filled with phantom elements on final structural dynamic model

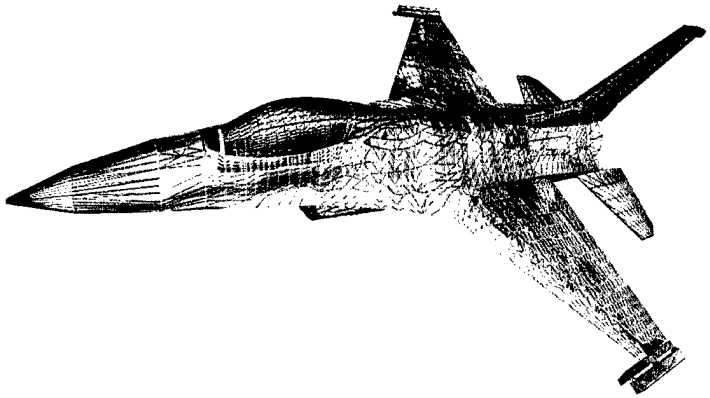

Figure 6.9: Final structural dynamic model

6.2 Euler Fluid Grid of the F-16

The aerodynamic portion of the simulations was computed using the Euler equations for invisid fluid dynamics. In order to accomplish these calculations it was first necessary to develop an Euler fluid grid. The first step toward accomplishing this was to obtain the Computer Aided Design (CAD) surface geometry of an F-16 Block 50 aircraft. The surface geometry shown in figure 6.10 was

provide by the Air Force Research Laboratory, Wright Patterson, with the help of contacts at the Air Force Flight Test Center at Edwards Air Force Base in California.

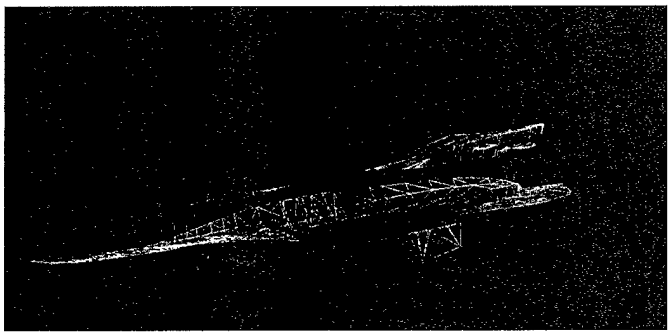

Figure 6.10: Computer Aided Design (CAD) Surface Geometry of an F-16 Block 50 Fighter Aircraft

Once the surface geometry was obtained a surface grid was developed as an intermediate step toward the full volume grid. Figure 6.11 shows the surface grid, and figure 6.12 shows the full volume grid, which has 403,919 grid points. This is the volume grid that was used for all of the simulations results presented in this document.

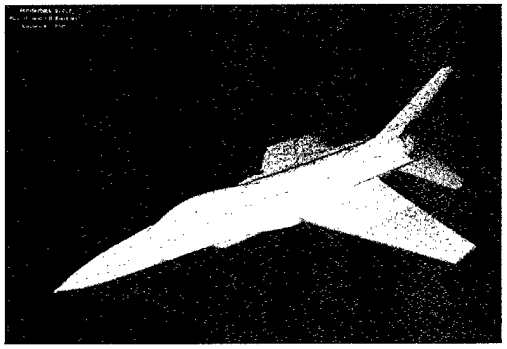

Figure 6.11: Surface Grid for the F-16 Block 50 Fighter Aircraft

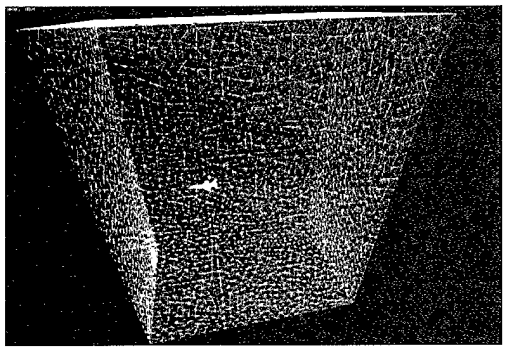

Figure 6.12: Volume Grid for the F-16 Block 50 Fighter Aircraft

6.3 Aeroelastic Numerical Solutions for the 3 Dimensional Model

Simulations of the full three-dimensional F-16 were conducted for Mach numbers of 0.7, 0.8, 0.9, 1.0, 1.1, 1.2, 1.3, and 1.4 at pressure and density values equivalent to 3000 M (10,000 ft). In order to validate the accelerated flutter flight testing approach accelerated test point at the same conditions and at an acceleration rate on 0.05 Mach/sec. Simulations were also conducted at elevated 3.5 and 5 g's in the normal direction in order investigate the effects of normal acceleration. The frequency and damping results of the simulation for the one g maneuvers was compared to the frequency and damping results for the flight test data shown in figure 6.13.

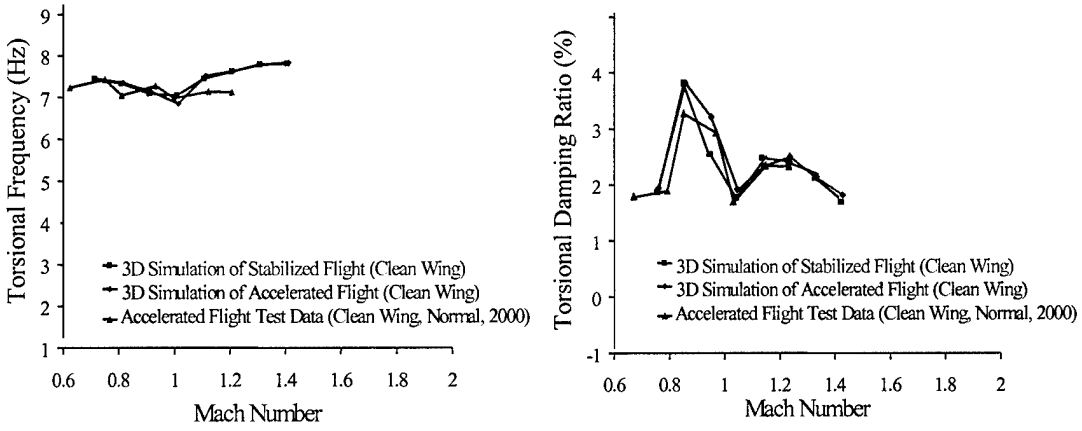

Figure 6.13 shows the correlation between the flight test data and the simulation data.

The frequency and damping results for the 3.5g and 5g flight test data were compared to frequency and damping results for the simulation data. Because the 3.5g and 5g flight test data were collected using the "wind up turn" technique (which is literally flying around in circles) the aircraft was flying into its own turbulence wake. As a result the data are somewhat noisy, and difficult to identify the frequency and damping. Consequently, one cannot expect the high g data to correlate as well with simulation data as was seen in the one g case. Although interpretation of the data are complicated by the turbulence encountered in the flight testing, the trend of the data should be conserved. The data shown in figure 6.14 compares the frequency and damping values for the 3.5g flight test data with frequency and damping values for the 3.5g simulation data. As one can observe, the frequency data correlates well, and the trend of the damping values is captured.

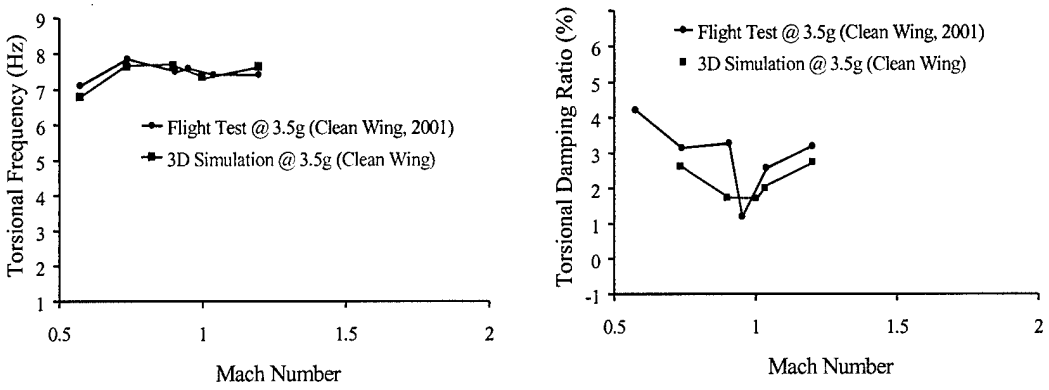

Figure 6.14: frequency and damping correlation between flight test data and simulation data for a 3.5g maneuver.

In figure 6.15 the frequency and damping plots for the 5g flight test data are compared to the frequency and damping plots for the 5g simulation results. Again the frequency plots agree very well, while the damping plots capture the trend.

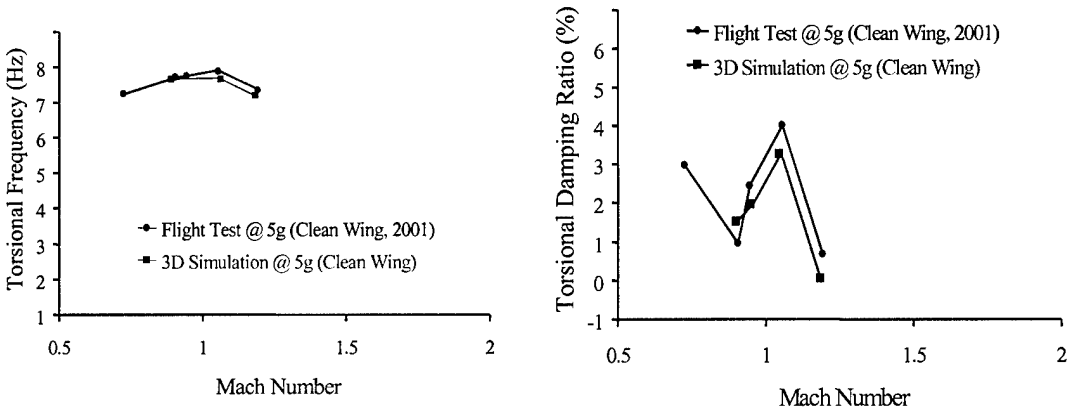

Figure 6.15: frequency and damping correlation between flight test data and simulation data for 5g.

Therefore, in every case, the aeroelastic parameters are insensitive to acceleration whether it is in the longitudinal or normal direction. It has also been shown that using the windowing technique and FastERA it is possible to identify the aeroelastic parameters from accelerating data, whether it comes from simulation or from flight test. It can also be concluded that for an F-16 fighter configuration

without external stores the simulations do a very good job of capturing the aeroelastic behavior of the actual aircraft even though physical phenomenon like viscosity and turbulence were not accounted for in the simulation. These phenomena would become more influential (especially viscosity) when simulating a configuration with external stores on the wings of the aircraft, or at higher angles of attack.

7.0 Real Time Predictive Analysis

In this chapter, the third issue is examined, namely "the need to anticipate the vibration response at airspeeds beyond which the aircraft has accelerated". In order to accomplish this an analytical study of an aeroelastic system will be performed. It would be untenable to consider an analytical study on the full aeroelastic system of the F-16 that has been presented in chapter 6. Therefore a simplified aeroelastic system will be considered for this study. These simplified models will only give an indicator of the stability of the system. They lack the fidelity to provide reliable predictive analysis. However what is needed to support knock-it-off decisions is an educated guess. As the flight test progresses the simplified models can be adjusted using feedback from the collected data. The adjusted model will provide an improved estimate for the stability of the system. Before the aircraft reaches the critical speed, the model should be refined enough to anticipate the danger, and the flight test can be halted. Historical results from flutter flight testing reveals that the flutter mechanisms on full scale aircraft have typically been dominated by one or two modes. Therefore only systems with one or two degrees of freedom will be considered in this study. These analytical studies will facilitate generalizations that can be made to the behavior of these systems. The results of this study can be used to develop rational criteria for when testing should be terminated.

7.1 The One Degree of Freedom System

The one degree of freedom system considered here is a typical two dimensional air foil that is free to move in rotation (equivalently: pitch or torsion) but is restrained from moving in plunge (equivalently: bending) as shown in figure 7.1.

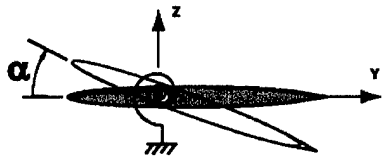

Fig 7.1: two dimensional airfoil with one (rotational) degree Of freedom.

7.1.1 Nomenclature

b – ½ chord

a – position of the center of axis measured from the simi-chord and divided by b (see fig. 7.2)

U – flight speed

h – bending displacement

α - rotational displacement

ρ_∞ - density

S – plan area = 2b for unit length wing section

k_α - torsional bending stiffness

φ - indicial function

I_α - rotational moment of inertia

M_y - Aerodynamic Moment acting on airfoil

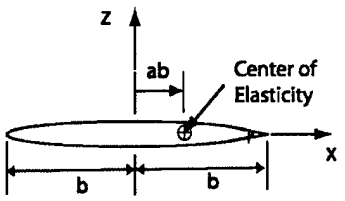

Fig 7.2: a is a nondimensional measure of the center of elasticity from the center chord such that –1 indicates the leading edge and 1 indicates the trailing edge

7.1.2 The One Degree of Freedom Mathematical Model

From Equation 6.143 on page 259 of Principles of Aeroelaticity [2] the equation of motion for a two dimensional airfoil allowed to move only in rotation as shown in figure 7.2 is as follows.

$$\left[I_\alpha + \frac{\pi}{2}\rho_\infty b^3 S\left(\frac{1}{8}+a^2\right)\right]\ddot{\alpha} - \frac{\partial M_y}{\partial \dot{\alpha}}\dot{\alpha} + \left[k_\alpha - \frac{\partial M_y}{\partial \alpha}\right]\alpha = 0 \qquad (7.1)$$

Also from Principles of Aeroelasticity [2]: equation 4.171 on page 120, the expression for the aerodynamic moment acting on a two dimensional airfoil allowed to rotate and plunge is as follows.

(7.2)

$$M_y(s) = \pi\rho_\infty b^2\left[ba\ddot{h} - Ub\left(\frac{1}{2}-a\right)\dot{\alpha} - b^2\left(\frac{1}{8}+a^2\right)\ddot{\alpha}\right]$$
$$+2\pi\rho_\infty Ub^2\left(\frac{1}{2}+a\right)\int_0^s \frac{d}{d\sigma}\left[\dot{h}(\sigma)+U\alpha(\sigma)+b\left(\frac{1}{2}-a\right)\dot{\alpha}(\sigma)\right]\varphi(s-\sigma)\,d\sigma$$

Where s is the distance in semichords traveled since $t = 0$. Specifically, $s = \frac{Ut}{b}$, and φ is the indicial function which is a dimensionless aerodynamic operator. This operator is not consistently defined in the literature, however 2π will cause the indicial function to asymptotically approach unity. φ has many forms depending on the flow regime, and the geometry of the aircraft. For more information on the indicial function refer to page 120 of reference [2].

It is assumed that the bending degree of freedom will be constrained to zero since only the torsional degree of freedom is allowed to move. This constraint is shown mathematically in equation (7.3).

$$h = \dot{h} = \ddot{h} = 0 \qquad (7.3)$$

Combining equations (7.2) and (7.3) yields the following equation.

(7.4)

$$M_y(s) = 2\pi\rho_\infty Ub^2\left(\frac{1}{2}+a\right)\int_0^s \frac{d}{d\sigma}\left[U\alpha(\sigma)+b\left(\frac{1}{2}-a\right)\dot{\alpha}(\sigma)\right]\varphi(s-\sigma)\,d\sigma$$
$$-\pi\rho_\infty b^2\left[Ub(\frac{1}{2}-a)\dot{\alpha}+b^2\left(\frac{1}{8}+a^2\right)\ddot{\alpha}\right]$$

Taking the derivative of the aerodynamic moment (equation (7.4)) with respect to rate of rotation of the airfoil ($\dot{\alpha}$) and taking into account that 2, π, ρ_∞, b, and U are all constant with respect to $\dot{\alpha}$ yields equation (7.5).

$$\frac{\partial M_y}{\partial \dot{\alpha}} = \left[2\pi\rho_\infty Ub^2\left(\frac{1}{2}+a\right)\right]\int_0^s U\varphi(s-\sigma)d\sigma - \pi\rho_\infty b^3U(\frac{1}{2}-a) \qquad (7.5)$$

Similarly taking the derivative with respect to α yields equation (7.6).

$$\frac{\partial M_y}{\partial \alpha} = \left[2\pi\rho_\infty U b^2 \left(\frac{1}{2} + a \right) \right] \int_0^s \dot{U} \varphi(s-\sigma) d\sigma \tag{7.6}$$

In summary equation (7.1) can be written as:

$$C_1 \ddot{\alpha} + C_2 \dot{\alpha} + C_3 \alpha = 0 \tag{7.7}$$

Where

$$C_1 = I_\alpha + \frac{\pi}{2} \rho_\infty b^3 S(\frac{1}{8} + a^2)$$

$$C_2 = \pi\rho_\infty b^3 U(\frac{1}{2} - a) - \left[2\pi\rho_\infty U b^2 \left(\frac{1}{2} + a \right) \right] \int_0^s U \varphi(s-\sigma) d\sigma$$

$$C_3 = k_\alpha - \left[2\pi\rho_\infty U b^2 \left(\frac{1}{2} + a \right) \right] \int_0^s \dot{U} \varphi(s-\sigma) d\sigma$$

Note that C_2 and C_3 are dependent on s which is itself dependent on time. Therefore these are time dependent coefficients.

Now, three particular cases will be considered where the indicial function will be set to zero, a constant, and an arbitrary function respectively.

Case I, where φ is zero, will be considered because it simplifies equation (7.7) making it a linear second order differential equation with constant coefficients, Studying this simple case will, hopefully give insight into the more complex case. Case II, where φ is constant, is a good approximation for supersonic flow with a thin airfoil. This case is being investigated because it includes real world complexity and therefore provides a more credible tool for extrapolating damping trends. Case III is clearly the most useful model, however it also the most complex, and will have to be solved numerically.

7.1.2.1 Case I: $\varphi = 0$

In case I, where φ is equal to zero, C_2 and C_3 can be simplified as follows.

$$C_2 = \pi \rho_\infty U b^3 (\frac{1}{2} - a)$$

$$C_3 = k_\alpha$$

Notice here that C_2 and C_3 are no longer dependent on time.

Since C_1 is non-zero equation (7.7) can be rewritten as:

$$\ddot{\alpha} + \tilde{C}_2 \dot{\alpha} + \tilde{C}_3 \alpha = 0 \qquad (7.8)$$

Where:

$$\tilde{C}_2 = \frac{C_2}{C_1}$$

and

$$\tilde{C}_3 = \frac{C_3}{C_1}$$

There are three sub-cases that must be considered. Sub-case I where

$$\tilde{C}_2^2 - 4\tilde{C}_3 > 0$$

Sub-case II where

$$\tilde{C}_2^2 - 4\tilde{C}_3 = 0$$

Sub-case III where

$$\tilde{C}_2^2 - 4\tilde{C}_3 < 0$$

For sub-case I the solution to equation (7.8) is:

$$\alpha = B_1 e^{\lambda_1 t} + B_2 e^{\lambda_2 t}$$

Where λ_1 and λ_2 are defined as follows.

$$\lambda_{1,2} = \frac{-\tilde{C}_2 \pm \sqrt{\tilde{C}_2^{\,2} - 4\tilde{C}_3}}{2}$$

If the initial conditions are $\alpha(t_0) = \alpha_0$ and $\dot{\alpha}(t_0) = \dot{\alpha}_0$ it can be shown that:

$$B_1 = \frac{\lambda_1 \alpha_0 - \dot{\alpha}_0}{\lambda_1 - \lambda_2}$$

$$B_2 = \frac{\lambda_2 \alpha_0 - \dot{\alpha}_0}{\lambda_2 - \lambda_1}$$

For sub-case II the solution for equation (7.8) is:

$$\alpha = B_1 e^{\lambda t} + B_2 t e^{\lambda t} = \left(B_1 + B_2 t\right) e^{\lambda t}$$

Where:

$$\lambda_1 = \lambda_2 = \lambda = \frac{-\tilde{C}_2}{2}$$

$$B_1 = \alpha_0$$

$$B_2 = \dot{\alpha}_0 - \lambda \alpha_0$$

For sub-case III the solution for equation (7.8) is:

$$\alpha = e^{-\frac{\tilde{C}_2}{2}t}(B_1 \cos \omega t + B_2 \sin \omega t)$$

Where:

$$\omega = \frac{\sqrt{\left|\tilde{C}_2^2 - 4\tilde{C}_3\right|}}{2}$$

$$B_1 = \alpha_0$$

$$B_2 = \dot{\alpha}_0 + \frac{\tilde{C}_2}{2}$$

The term $(B_1 \cos \omega t + B_2 \sin \omega t)$ is bounded so the stability, in this case, depends on the $e^{-\frac{\tilde{C}_2}{2}t}$ term. The stability of this term also depends on the sign of $\tilde{C}_2$.

Reference [17] shows the term $e^{-\frac{\tilde{C}_2}{2}t}$ in the form $e^{-\zeta\omega_n t}$ where ζ is the damping, and ω_n is the natural frequency. This result will come in handy later in this chapter.

It is also worth noting that, in the case that φ is zero, $\lambda_1\lambda_2 = \tilde{C}_3$ and $\lambda_1 + \lambda_2 = -\tilde{C}_2$. In other words, if $\tilde{C}_3$ is positive then the sign of λ_1 will be the same as the sign of λ_2 and will be opposite sign of $\tilde{C}_2$. One can see that $\tilde{C}_3$ is positive, so λ_1 will have the same sign as λ_2. The sign of λ_1

and λ_2 will be opposite the sign of $\tilde{C}_2$ which can be determined by the term $\frac{1}{2}-a$. Therefore one can conclude that λ_1 and λ_2 are negative if and only if $a<\frac{1}{2}$. Therefore the airfoil will be stable if and only if the center of elasticity is forward of the $\frac{3}{4}$ chord.

So for case 1 ($\varphi=0$) the solution and therefore the frequency and damping values are directly attainable. Now consider case 2 where φ = constant which will give results that are more representative of actual aeroelastic systems.

7.1.2.2 Case II: φ = constant

This case is of limited practical use because φ is only a constant at supersonic speeds, but it is a real physical case and can give insight to the behavior of aeroelastic systems in general.

$$C_1 = I_\alpha + \frac{\pi}{2}\rho_\infty b^3 S(\frac{1}{8}+a^2)$$

$$C_2 = \pi\rho_\infty b^3 U(\frac{1}{2}-a) - \left[2\pi\rho_\infty U^2 b^2\left(\frac{1}{2}+a\right)\right]\varphi s$$

$$C_3 = k_\alpha$$

Notice here that C_2 is dependent on time but C_3 is not. This leads to an equation of the form:

$$\ddot{\alpha} + (d_1 + d_2 s)\dot{\alpha} + d_3\alpha = 0 \qquad (7.9)$$

Where:

$$d_1 = \frac{\pi\rho_\infty b^3 U\left(\frac{1}{2} - a\right)}{C_1} \qquad (7.10)$$

$$d_2 = \frac{2\pi\rho_\infty U^2 b^2\left(\frac{1}{2} + a\right)\varphi}{C_1} \qquad (7.11)$$

and

$$d_3 = \frac{k_\alpha}{C_1} \qquad (7.12)$$

The obvious approach to getting a solution for equation (7.9) is to use a series solution. This approach was investigated and found to not lead to a closed form solution. The next approach that was tried was reformulating the problem as a system of first order equations, and finding an estimator on α that would bound the actual amplitude.

Rearranging equation (7.9) yields:

$$\ddot{\alpha} = -(d_1 + d_2 s)\dot{\alpha} - d_3\alpha \qquad (7.13)$$

Next define

$$z_1 = \alpha$$
$$z_2 = \dot{\alpha} \tag{7.14}$$

Taking the derivative of equations (7.14) and combining with equation (7.13) yields:

$$\dot{z}_1 = \dot{\alpha} = z_2$$
$$\dot{z}_2 = \ddot{\alpha} = -d_3 z_1 - (d_1 + d_2 s) z_2 \tag{7.15}$$

Now define

$$z = \begin{bmatrix} z_1 \\ z_2 \end{bmatrix} \tag{7.16}$$

Then rewrite equations (7.15) as:

$$\dot{z} = \begin{bmatrix} 0 & 1 \\ -d_3 & -(d_1 + d_2) \end{bmatrix} z \tag{7.17}$$

Next define:

$$w = (z_1^2 + z_2^2)^{1/2} \tag{7.18}$$

Taking the derivative of equation (7.18) gives:

$$\dot{w} = \frac{1}{2}(z_1^2 + z_2^2)^{-1/2}(2z_1\dot{z}_1 + 2z_2\dot{z}_2) = \frac{z_1\dot{z}_1 + z_2\dot{z}_2}{w} \tag{7.19}$$

Recalling equations (7.15) it can be seen that:

$$\dot{w} = \frac{z_1 z_2 + z_2(-d_3 z_1 - (d_1 + d_2 s) z_2)}{w} = \frac{(1-d_3)z_1 z_2 - (d_1 + d_2 s) z_2^2}{w} \tag{7.20}$$

Consider the term

$$(1-d_3)z_1 z_2 - (d_1 + d_2 s) z_2^2$$

It is easy to see that:

$$(1-d_3)z_1 z_2 - (d_1 + d_2 s) z_2^2 \le \left|(1-d_3)z_1 z_2 - (d_1 + d_2 s) z_2^2\right| \tag{7.21}$$

From equation (7.21) and the triangle inequality one can see that:

$$\left|(1-d_3)z_1 z_2 - (d_1 + d_2 s) z_2^2\right| \le \left|(1-d_3)\right|\left|z_1\right|\left|z_2\right| + \left|(d_1 + d_2 s)\right| z_2^2 \tag{7.22}$$

Now consider the quantity:

$$\left(|z_1| - |z_2|\right)^2 \ge 0$$

$$z_1^2 - 2|z_1 z_2| + z_2^2 \ge 0$$

$$z_1^2 + z_2^2 \ge 2|z_1 z_2|$$

This result and inequality (7.22) to conclude leads to the conclusion that:

(7.23)

$$\left|(1-d_3)\right|\left|z_1\right|\left|z_2\right|+\left|\left(d_1+d_2 s\right)\right|z_2^2 \le \left(\frac{\left|1-d_3\right|}{2}+\left|\left(d_1+d_2 s\right)\right|\right)w^2$$

Combining the inequalities (7.21) (7.22) (7.23) with equation (7.20):

$$\dot{w} \le k(s)w$$

Where

$$k\left(s\right)=\frac{\left|1-d_3\right|}{2}+\left|\left(d_1+d_2 s\right)\right| \qquad (7.24)$$

Now apply Gronwall's lemma [15].

$$\left|w\right| \le \left|w_0\right| e^{\int_{s_0}^{s} k(s)d\tau} \qquad (7.25)$$

Where

$$w_0 = w\left(s_0\right)$$

Recalling equations (7.18) and (7.24) equation (7.25) becomes:

$$\left|(z_1^2+z_2^2)^{1/2}\right| \le \left|(z_1^2(s_0)+z_2^2(s_0))^{1/2}\right| e^{\int_{s_0}^{s}\left(\frac{|1-d_3|}{2}+|(d_1+d_2 s)|\right)d\tau}$$

Recalling equation (7.14) gives:

$$\left|(\alpha^2+\dot{\alpha}^2)^{1/2}\right| \le \left|(\alpha_0^2+\dot{\alpha}_0^2)^{1/2}\right| e^{\int_{s_0}^{s}\left(\frac{|1-d_3|}{2}+|(d_1+d_2 s)|\right)d\tau}$$

From this it can be deduced that:

$$|\alpha| \le \left|(\alpha_0^2+\dot{\alpha}_0^2)^{1/2}\right| e^{\int_{s_0}^{s}\left(\frac{|1-d_3|}{2}+|(d_1+d_2 s)|\right)d\tau} \qquad (7.26)$$

Equation (7.26) is a bound on the solution to equation (7.9), which represents the system that is under investigation.

It would be beneficial to have some estimate of the damping of the system, but the estimation gives us a bound on α. In order to get an estimate of damping it is necessary to make some assumptions, because damping is really associated with a linear system, and the system under investigation is nonlinear. However, an exponential bound has been developed for the system:

$$e^{\int_{s_0}^{s}\left(\frac{|1-d_3|}{2}+|(d_1+d_2 s)|\right)d\tau}$$

That resembles the exponential bound seen in case I, sub-case III. Recalling that reference [17] gives the solution in the form.

$$e^{-\zeta\omega_n t}$$

So if the exponent is divided by $-\omega_n t$ all that remains is the damping term. If it is further assumed that $\omega_n \cong \omega$ where ω is the damped frequency then the following formula will give us an estimate of damping.

$$\zeta = -\frac{\int_{s_0}^{s}\left(\frac{|1-d_3|}{2}+|(d_1+d_2 s)|\right)d\tau}{\omega}$$

It turns out that this approach is extremely conservative. That is because the system that is being considered can be divergent, stable, or convergent, and the estimator implicitly assumes the worst case, that is that the system is divergent.

A numerical study is performed in section 7.4 that shows this is indeed the case.

7.1.2.3 Case III: φ is arbitrary

In the case that φ is arbitrary any form of the indicial function can be used. With increased complexity an analytical solution becomes harder to come by. However, a numerical solution can always be reached, and this numerical solution can be used to anticipate the damping at airspeeds not yet reached, and aid in making the knock-it-off decisions that sometimes have to be made during flutter flight testing.

7.1.3 Numerical Study of the One Degree of Freedom Error Analysis

In order to assess the utility of the estimator (equation (7.26)) for the one-degree of freedom system, a MATLAB SIMULINK model was built (shown in figure 7.3) that includes the one-degree of freedom system, the estimator, and a comparison between the two. The green portion of the model is the one-degree of freedom system that will numerically solve equation (7.9). The blue portion of the model is the estimator, which calculates the right side of equation (7.26). The red portion of the model simply calculates the ratio of the outcome of the one-degree of freedom system and the estimator. Results are presented for two cases in figures 7.4 and 7.5. The parameters used for each case can be found in Table 7.1.

The first case represents a set of parameters that are not physically relevant and include a very small chord length and very low airspeed. These parameters were selected such that the estimator would perform well. The data for case I are shown in figure 7.4. One can see from the figure that the stability of the system is driven by the location of the center of elasticity. If the center of elasticity is forward of the quarter chord the system is unstable. If the center of elasticity is aft of the quarter chord the system is stable. This is driven by d_2 term described in equation (7.11). Specifically if the term (½+a) is negative the system will be stable. It can also be seen in the graph that the estimator predicts the system will be unstable, and the only time the estimator is very close to the simulation is when a = -½. One final observation is that as the airspeed (U) increases the estimator becomes increasingly more conservative.

The second case represents a more realistic geometry, however, as one might expect from the trends observed in the first case, the estimator is ridiculously conservative when the chord length and the airspeed are more realistic. The second case is illustrated in figure 7.5.

One positive thing that can be said for the estimator is that in all cases it bounds the simulation data perfectly.

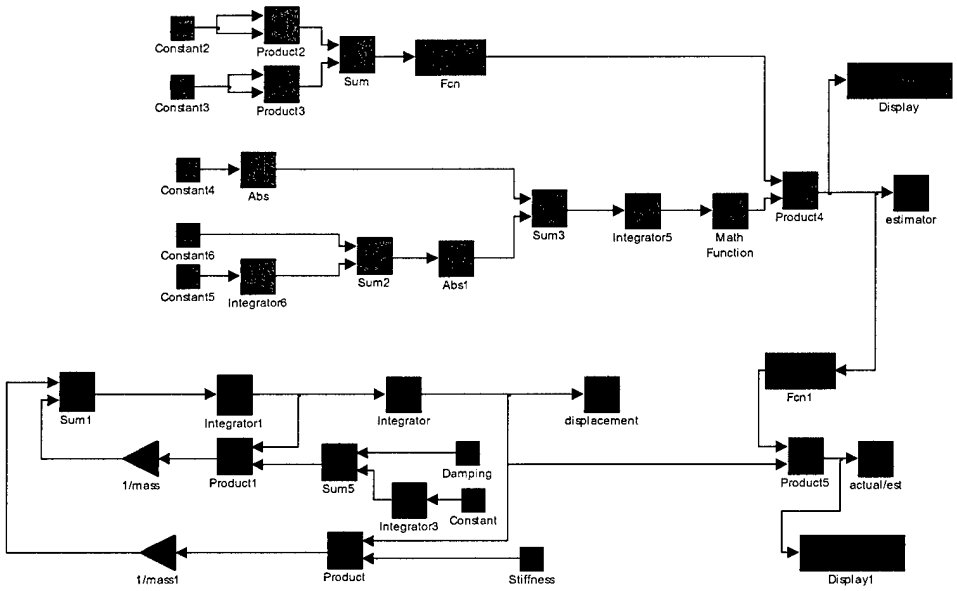

Figure 7.3: Matlab Simulink model used to simulate the one degree of freedom system (green), estimator (blue), and the comparison between the two (red).

Table 7.1: Parameter values for two cases presented for 1 degree of freedom error analysis numerical study.

	Stable Good Estimator	Estimator for a Realistic System
Parameter	Case 1	Case 2
U (mph)	10 through 100	100 through 300
Rho	0.001	0.001736
I_alpha	0.001	0.5522
B	0.005	1.0
S	0.01	2.0
A	0.0 through –1.0	-0.49 through –0.56
K_alpha	0.001	345.1
Gamma	1.4	1.4
Pressure	0.001	1455.7

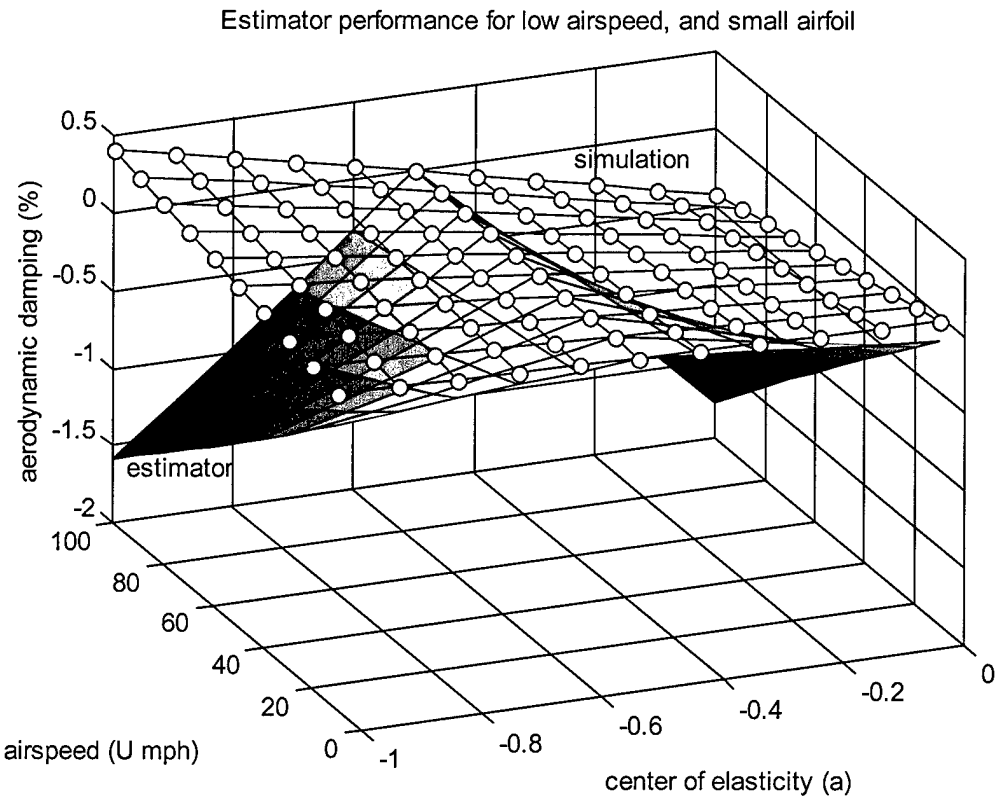

Figure 7.4: Comparison of damping results for the estimator and simulation of the one degree of freedom airfoil with a small chord length and low airspeeds.

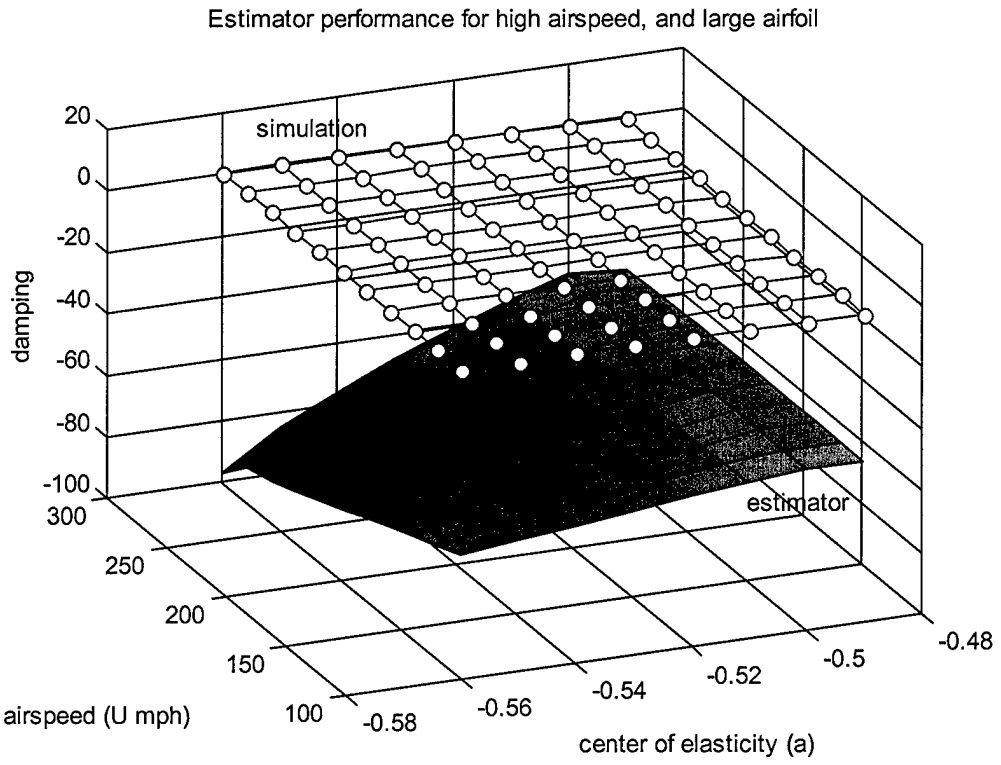

Figure 7.5: Comparison of damping results for the estimator and simulation of the one degree of freedom airfoil with a larger chord length and higher airspeeds.

7.1.4 Symbolic Solution to the One Degree of Freedom System

A solution to equation (7.13) can be found using a symbolic math solver. The symbolic math solver in Matlab was used for this purpose. The resulting solution is shown in equation.

(7.27)

$$\alpha = \frac{e^{-1/4t(d_2t+2d_1)}}{\left(\frac{d_1+d_2t}{d_2^{1/2}}\right)}\left[C_1W\left(\frac{1}{4}\left(\frac{-d_2+2d_3}{d_2}\right),\frac{1}{4},\frac{1}{2}\left(\frac{(d_1+d_2t)^2}{d_2}\right)\right)+C_2M\left(\frac{1}{4}\left(\frac{-d_2+2d_3}{d_2}\right),\frac{1}{4},\frac{1}{2}\left(\frac{(d_1+d_2t)^2}{d_2}\right)\right)\right]$$

Where W and M are Whittaker functions. Whittaker functions are confluent hypergeometric functions that are defined below [16].

$$M(k,m,z) = e^{-z/2} z^{m+1/2} {}_1F_1\left(\tfrac{1}{2}+m-k, 1+2m, z\right) \tag{7.28}$$

$$W(k,m,z) = e^{-z/2} z^{m+1/2} U\left(\tfrac{1}{2}+m-k, 1+2m, z\right) \tag{7.29}$$

Where ${}_1F_1$ and U are also confluent hypergeometric functions known as Kummer's functions. Kummer's functions are defined below [16].

$${}_1F_1(a;b;z) = 1 + \frac{a}{b}z + \frac{a(a+1)}{b(b+1)}\frac{z^2}{2!} + \ldots = \sum_{k=0}^{\infty} \frac{(a)_k}{(b)_k}\frac{z^k}{k!} \tag{7.30}$$

Where $(a)_k$ and $(b)_k$ are Pochhammer symbols [16].

$$U(a,b,z) = \frac{1}{\Gamma(a)} \int_0^{\infty} e^{-zt} t^{a-1} (1+t)^{b-a-1}\, dt \tag{7.31}$$

Where $\Gamma(a)$ is the gamma function [16], which extends the factorial function to complex and real numbers.

Combining equations (7.27) through (7.31) results in the following:

$$\alpha = \frac{e^{-1/4t\left(d_2 t + 2d_1\right)}}{\left(\frac{d_1 + d_2 t}{d_2^{1/2}}\right)} \left[C_1 e^{-z/2} z^{\tilde{m}+1/2} \frac{1}{\Gamma(a)} \int_0^\infty e^{-zt} t^{\tilde{a}-1} \left(1+t\right)^{\tilde{b}-\tilde{a}-1} dt + C_2 e^{-z/2} z^{\tilde{m}+1/2} \left(1 + \frac{\tilde{a}}{\tilde{b}} z + \frac{\tilde{a}\left(\tilde{a}+1\right)}{\tilde{b}\left(\tilde{b}+1\right)} \frac{z^2}{2!} + \ldots \right) \right]$$

Where:

$$\tilde{k} = \frac{1}{4}\left(\frac{-d_2 + 2d_3}{d_2} \right)$$

$$\tilde{m} = \frac{1}{4}$$

$$\tilde{z} = \frac{1}{2}\left(\frac{\left(d_1 + d_2 t\right)^2}{d_2} \right)$$

$$\tilde{a} = \frac{1}{2} + \tilde{m} - \tilde{k} = 1 - \frac{1}{2}\frac{d_3}{d_2}$$

and

$$\tilde{b} = 1 + 2\tilde{m} = \frac{3}{2}$$

So given an exact solution to the one degree of freedom typical wing section it will be possible to project the motion of the airfoil to any airspeed or Mach number as needed to support knock-it-off decisions in the control room. A word of caution is in order here; this solution is based on a very simple model and should not be expected to yield results that are predictive in nature. This is only intended to yield ballpark estimates that can be used to support real-time decision making.

7.2 Knock-it-off Criteria & Real Time Displays

The final issue that needs to be considered is the knock-it-off criteria. Figures 7.6 through 7.8 depict a conceptual scenario for accelerated flutter testing. In figure 7.6 the black predicted damping curve would come from the high fidelity simulations that would be conducted prior to the flight testing. The red curve, labeled "predicted damping adjusted for uncertainty", is shown here as simply transposition of the original predicted curve. In principle, it could be a more complex adjustment of the original predicted damping curve that accounts for the measured damping values that are collected during the flight, and the uncertainties that are present in all such tests. The red line at the bottom of the chart that is labeled "critical damping" represents the damping value that the program will not break intentionally. Because the parameter identification of data from an accelerating aircraft will add an additional uncertainty, a new line labeled "accelerated critical damping" will be used as a "must not break" line. The left edge of the blue vertical band represents the Mach number at the current moment in time. Conceptually this band will move across the display from left to right as the aircraft accelerates. The right edge of this blue band represents the expected Mach number that will occur three seconds from the current time. The width of the blue band will be wider at higher acceleration rates and narrower at lower acceleration rates. The blue tangent line that is shown represents a projection of the damping trend that can lead to a projected flutter speed. This could be accomplished using the tangent line as shown, or other technique such as the flutter-o-meter concept developed at NASA Dryden [18], or the Zimmerman method [19].

In figure 7.7 the projected flutter speed has reached right hand side of the band representing the anticipated Mach number three seconds from the present time. The band has turned yellow to emphasize the problem. At this point a real potential exists that the aircraft could exceed the flutter speed before data can be analyzed and control room engineers and aircraft crew can react to avoid the

disaster [20,21]. One solution to this dilemma is to simply reduce the acceleration rate as shown in figure 7.8. In an extreme case the acceleration rate could be reduced to zero, in which case the accelerated flutter test technique would then degenerate into the conventional stabilized flutter test technique.

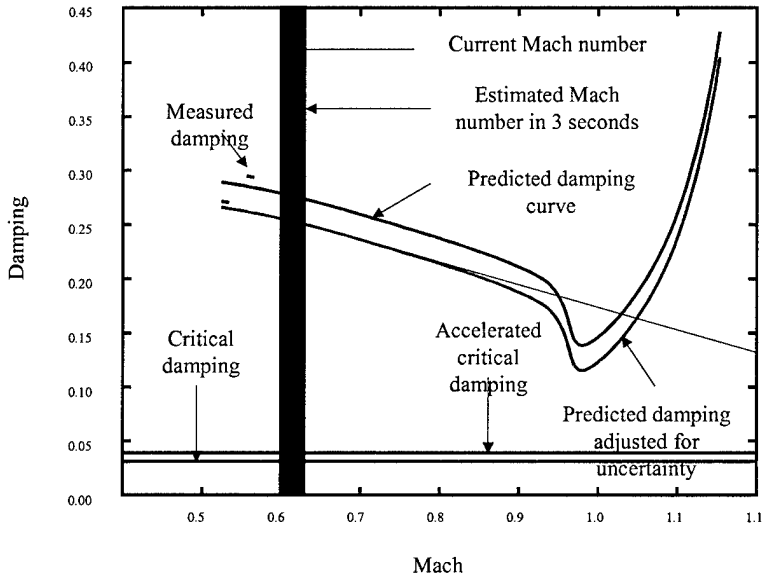

Figure 7.6: Proposed accelerated flutter testing display, and methodology.

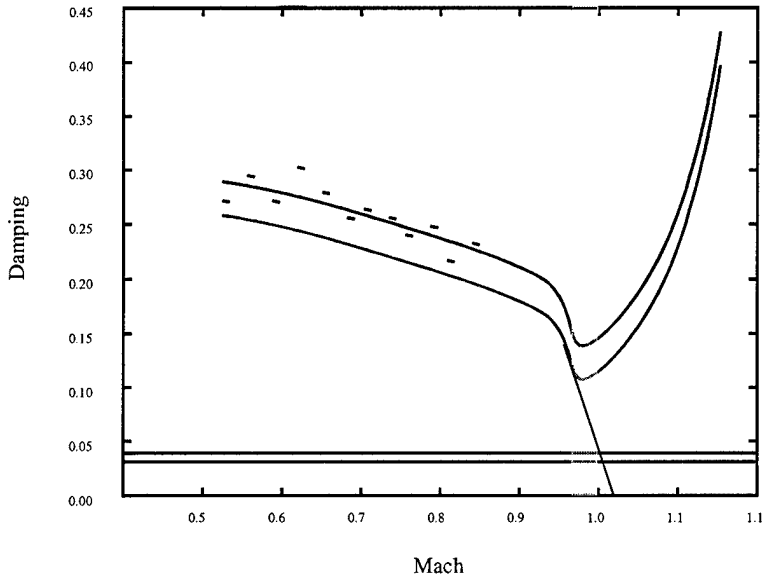

Figure 7.7: Accelerated flutter testing acceleration rate must be reduced or halted to avoid unreasonable risk.

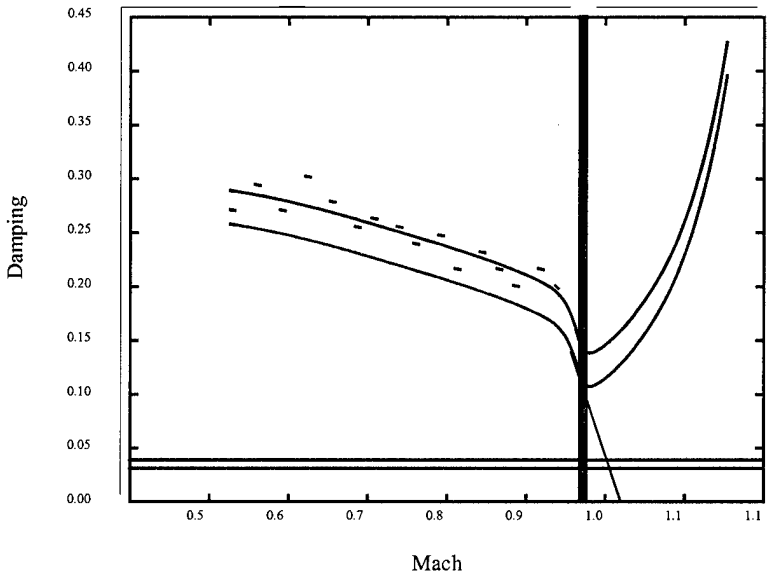

Figure 7.8: Accelerated flutter testing reaches a point where acceleration rate must be reduced or halted.

The hope in conducting the research in sections 7.1 and 7.2 was to develop a method by which damping could be predicted at Mach numbers higher than had been flown, that would be reasonable (in the ball park) and conservative. These predictions could then be used to develop the adjusted predictive analysis, or perhaps the projected flutter speed to be used in the knock-it-off criteria. For the purpose of this section we will focus on the one degree of freedom equations developed in section 7.1 because the flutter mechanism in the F-16 data that we have examined so far is in fact a one degree of freedom flutter mechanism. In figure 7.9 the numerical solution of equation (7.9), which is equivalent to the exact solution presented in equation (7.27) is compared to the two degree of freedom model of the F-16 developed in chapter 4. Notice that at the high Mach number the system does a very good job of predicting the damping of the system, and recall that the indicial function used to develop equation (7.9) was for the supersonic case. When compared to the 3 dimensional flight test results (7.9) it can be seen for this case the indicial function estimator agrees well with the flight test for the supersonic condition, and is conservative for the lower airspeeds.

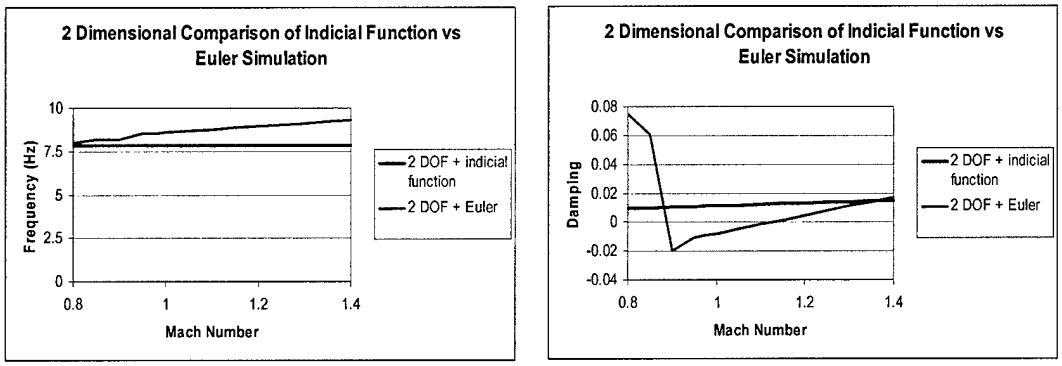

Figure 7.9: Frequency and Damping Comparison Between Indicial Function and Euler Simulation for a 2 Degree of Freedom Typical Wing Section Representation of the F-16.

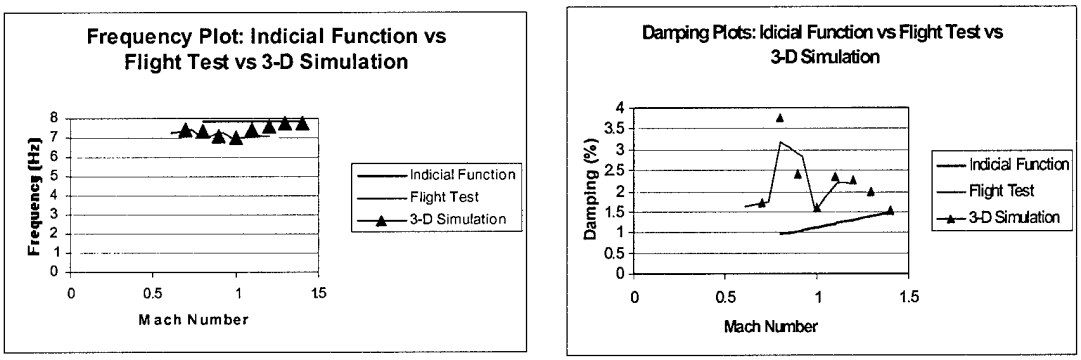

Figure 7.10: Frequency and Damping Comparison Between Indicial Function, 3-Dimensional Simulation, and Flight Test Data for the F-16.

8.0 Conclusions

Section 1.6 outlined several issues that would need to be addressed in order to develop the accelerated flutter test technique. For convenience these issues are summarized below.

1) The first issue is whether or not the frequencies and dampings are affected by the acceleration of the aircraft.

2) The second issue is whether or not parameter identification algorithms can extract frequency and damping values from the time varying data.

3) The third issue is the need to anticipate the vibration response at airspeeds (or Mach numbers) beyond which the aircraft has accelerated.

4) The fourth issue is developing formal criteria to determine when the aircraft needs to end the acceleration and terminate the test point.

The first of these issues is addressed in chapter 3. In that chapter it was shown that there are inertial effects that mathematically change the basic aeroelastic system that is being investigated. These inertial effects change not only the forcing function acting on the aircraft, but also change the stiffness of the torsional degree of freedom of the typical wing section. At first glance this would appear to invalidate the accelerated flutter testing approach, however for typical aircraft geometries and performance the change in the torsional stiffness (and therefore the flutter parameters) will be very small (less than 0.2% for the F-16 case investigated). Specifically, the position of both the center of gravity and the center of elasticity are normally contained within the wing of the aircraft and within about one quarter chord of each other. This limits the moment arm that the inertial forces due to

acceleration can act upon. Also, for level acceleration, the acceleration of a high performance aircraft is likely less than 0.01 Mach/sec, which limits the magnitude of the inertial force due to the acceleration of the aircraft. Because the change in flutter parameters is negligible it is reasonable to expect the accelerated flutter test procedures to yield essentially the same results as the traditional stabilized flight test technique, assuming the parameters can be accurately identified using the data from an accelerating aircraft.

Therefore it can be concluded that the effect of acceleration on the flutter parameters is negligible for normal geometries and acceleration rates.

The second issue is addressed in chapter 4. In that chapter it was shown that the wet frequencies and damping ratios of an aircraft are functions of the free-stream Mach number. Therefore, during an accelerated flight, these parameters become time-dependent. For this reason, theory suggests that standard signal processing techniques, which are limited to time-invariant systems, cannot be applied to the identification of an accelerated aeroelastic system. However, within a time-window of 0.2 second, and for a typical level flight acceleration of 1 g or 0.03 Mach/second, the Mach number varies by 0.6% only. Hence, within a time-window of 0.2 second, the aeroelastic parameters of an accelerating aircraft can be assumed to remain constant. Such a time-window corresponds to 2 cycles of a mode at 10 Hz, a frequency that is relevant to the first bending and torsion modes of most aircraft. Therefore, any signal processing technique that can identify correctly a mode from 2 cycles of its response is a candidate technique for identifying the parameters of an accelerated aeroelastic system in a window by window approach. Furthermore, the analytical study typical wing section shows that realistic level flight accelerations do not affect the frequencies and damping ratios of an aero elastic system. In other words, the aeroelastic parameters of an aircraft identified during an accelerated flight are the same as those identified in stabilized flight conditions. Therefore flutter testing could be performed in accelerated flight, thereby reducing the cost and risk involved in determining the flutter envelopes of fighters. In practice, technical details such as re-excitation procedures, real-time identification, and flutter early alert systems must be addressed to enable such a technology.

Therefore it can be concluded that windowing can be used effectively to identify the parameters using data from an accelerating aircraft.

The third issue was addressed in chapter 7, namely, the need to anticipate the vibration response at airspeeds (or Mach numbers) beyond which the aircraft has accelerated. One key to safely using the accelerated flutter test method is the development of a predictive tool that can determine stability or the flutter speed of the system using subcritical flight test data. This chapter introduced the one degree of freedom system and explored different approaches to developing a predictive tool. The first approach was to develop an estimator that would conservatively predict the angle of attack of the one degree of freedom system. This estimator was found to be overly conservative, and of no practical use. The next approach was to find a direct solution of the one degree of freedom system. This approach naturally produced a perfect fit of the one degree of freedom system, and also did an excellent job of predicting the result of a simulation of the two degree of freedom typical wing section. However when considering the stability of a three dimensional system the simple predictor proves to be less than useful. This is an area where further research is needed. Among the potential solutions to this problem are three dimensional analytical models, reduced order models, or full three dimensional simulations could be used as the predictive tool. Ideally whatever predictive tool is used it should be updated using flight test data as it becomes available. Although this issue merits more research before it is used for live flutter testing, it has been demonstrated for a simple system that a simplified model can be used to predict flutter parameters conservatively.

Therefore it can be concluded, at least in principal, a simplified model of an aeroelastic system can be used to conservatively anticipate the damping at airspeeds higher than the currently attained airspeed.

The final issue was also addressed in chapter 7, that is developing formal criteria to determine when the aircraft needs to end the acceleration and terminate the test point. These criteria must allow

some time for aircraft excitation (if decay data is to be used) data to be collected and analyzed and corrective action taken. The biggest contributors to the time required for this chain of events are aircraft excitation which takes about 1 second, data collection which could take up to one second for noisy data, and reaction times for the engineer and the pilot which takes about one half second each. Although this three seconds could be reduced to one second if concurrent excitation and analysis is used and the engineer and pilot are taken out of the loop, it was shown in this chapter that using the three second criterion the aircraft could still be halted in time to avert a flutter situation. The Knock-It-Off criteria must also account for the uncertainty in the flight test data, and analysis methods, as well as the uncertainty results from the accelerating flight test procedure. This chapter also proposed a method of handling the uncertainties associated with open air flight testing in a conservative way.

Therefore it can be concluded, given that damping can be conservatively anticipated for higher airspeeds, the aircraft acceleration can be halted in time to avoid entering a flutter condition.

After exploring each of the issues above, it still appears that the accelerated flutter test technique is a viable approach to conducting flutter envelope expansion flight testing. There are still several research issues that need to be explored before this method is used to support initial flutter testing for a new aircraft. In the next chapter some of the supporting research that need to be accomplished are presented.

9.0 Future Work

9.1 Improved Damping Predictor/Estimator

One of the keys to successfully implementing the accelerated flutter testing capability is to have a reliable predictor for the damping values. For the first implementation the results from the full three-dimensional model could be used. However this approach provides predictive data for the test points as they are planned, but not necessarily how they are flown. These slight differences in altitude, or center of gravity location add to the uncertainty that already exists. The ideal predictor/estimator would be capable of providing predicted damping values for the aircraft in the configuration and conditions as flown in near real time. One approach to accomplishing this is through the use of Reduced Order Modeling which is discussed in section 9.2.

9.2 Reduced Order Modeling

Ideally the high fidelity 3 dimensional model would be used to run real time simulations to support flight test decisions with near real time estimates for the maneuvers as flown as opposed to as planned. However existing compute resources are not adequate to run the model anywhere near real time. It is still desirable to have reliable results to compare to flight test data. One method of reaching these results in a timely manner is to use a reduced order model. In order to develop the reduced order model the results of the full order model are needed. The algorithm uses these results to estimate a

reduced order system that produces the same observable dynamics within the allowable error bound as the full order model. The reduced order model is computationally much less expensive and will therefore run very near real time.

9.3 Flight Test Data Based Predictor/Estimator

Even though the full order model is very high fidelity, and therefore can do an excellent job of predicting the dynamics of the aircraft as designed, or as represented in the model, there will always be discrepancies between the model as designed (or modeled) and the real article as built. Because of this discrepancy, the simulation data is always somewhat suspect until it is validated with flight test data. However, occasionally the validation process will only reveal the discrepancy between the model and the real article. It is in this case that it is desirable to update the model such that it more accurately reflects the dynamics observed through flight test. Regardless of whether the model is the full order model or the reduced order model, if it is being used to predict or estimate the behavior of the aircraft at higher Mach numbers than has been achieved through flight test, it is critical that the model reflect the real life dynamics.

9.4 Evaluate Other Parameter Identification Methods

Eigensystem Realization Algorithm was used exclusively to perform parameter identification in this thesis. There are many other state space parameter identification algorithms that may perform as well or better than ERA for the aircraft flutter application. Although ERA has met the initial requirements it would be prudent to extend the investigation to other parameter identification methods. Areas in which ERA could be significantly improved upon are,

1) Concurrent excitation and analysis

2) Forgetting factor

3) Noise tolerance

Concurrent excitation and analysis enable the flight test engineer to use data that is collected during the excitation of the aircraft to perform the parameter identification. This would shorten the time required to look ahead and would also provide nearly continuous damping estimations as the aircraft accelerates. Both of these effects would improve the safety of conducting accelerating flutter testing.

A forgetting factor weights the data points at the end of the window more heavily than the data points at the beginning of the window. The weighting should allow the parameters to be identified more closely to the end of the window which would reduce the lag time between the time the parameter represents and the time the result is available to make decisions.

ERA performed reasonably with regard to noise tolerance, however it required five times as much data (0.2 seconds for clean data vs. 1.0 seconds for noisy data) to identify parameters from noisy data. The ability to identify parameters using a smaller window of data will improve the safety, and/or the efficiency of the accelerated flutter test technique.

9.5 Refine Knock-It-Off Criteria

The Knock-It-Off criteria presented in chapter 7 contains the essential characteristics that are necessary to support initial flutter testing on a new aircraft. These criteria provide a good outline but need to be further developed by soliciting requirements from the flutter flight test community. Clearly the final Knock-It-Off criteria should incorporate the improved damping predictor/estimator discussed above. It would also be helpful to develop statistical basis for evaluating the effect that noise has on

the uncertainty of the damping value identified from the flight test data. However, it may be difficult to attain enough data to do any kind of statistical analysis.

References

1 I. E. Garrick and Wilmer H. Reed III, Historical Development of Flutter, AIAA Paper 81-0591, AIAA/ASME/ASCE/AHS 22nd Structures, Structural Dynamics and Materials Conference, Atlanta, Ga., April 6-8, 1981.

2 R. L. Bisplinghoff and H. Ashley, Principles of Aeroelasticity, Dover Publication, New York, 1975.

3 J. N. Juang and R. S. Pappa, An Eigensystem Realization Algorithm (ERA) for Modal Parameter Identification and Model Reduction, J. of Guidance, Control, and Dynamics 1985, 8:620-627.

4 L. D. Peterson, Efficient Computation of the Eigensystem Realization Algotithm, J. Guidance, Control, and Dynamics 1995, 18:395-403.

5 L. D. Peterson, S. J. Bullock and S. W. Doebling, The Statistical Sensitivity of Experimental Modal Frequencies and Damping Ratios to Measurement Noise, Internat. J. of Anal. Exp. Modal Anal. 1996, 11:63-75. AIAA, Aerospace Sciences Meeting and Exhibit, 37th, Reno, NV, Jan 11-14, 1999.

6 L. Fezoui and B. Stoufflet, A Class of Implicit Upwind Schemes for Euler Simulations with Unstructured Meshes, J. Comp. Phys. 1989, 84:174-206.

7 C. Farhat, L. Fezoui, and S. Lanteri, Two-Dimensional Viscous Flow Computations on the Connection Machine: Unstructured Meshes, Upwind Schemes, and Massively Parallel Computations, Comput. Meths. Appl. Mech. Engrg. 1993, 102:61-88.

8 C. Farhat and S. Lanteri, Simulation of Compressible Viscous Flows on a Variety of MPPs: Computational Algorithms for Unstructured Dynamic Meshes and Performance Results, Comput. Meths. Appl. Mech. Engrg. 1994, 119:35-60.

9 R. Nkonga and H. Guillard, Godunov Type Method on Non-Structured Meshes for Three-Dimensional Moving Boundary Problems, Comput. Meths. Appl. Mech. Engrg. 1994, 113::183-204.

10 B. Koobus and C. Farhat, Second-Order Time-Accurate and Geometrically Conservative Implicit Schemes for Flow Computations on Unstructured Dynamic Meshes, AIAA Paper 98-0113, 36th Aerospace Sciences Meeting and Exhibit, Reno, Nevada, January 12-15, 1998.

11 B. Koobus and C. Farhat, Second-Order Time-Accurate and Geometrically Conservative Implicit Schemes for Flow Computations on Unsturctured Dynamic Meshes, Comput. Meths. Appl. Mech. Engrg. 1999, 170:103-130.

12 M. Lesoinne and C. Farhat, A Higher-Order Subiteration Free Staggered Algorithm for Nonlinear Transient Aeroelastic Problems, AIAA J. 1998, 36:1754-1757.

13 J. Donea, An Arbitrary Lagrangian-Eulerian Finite Element Method for Transient Fluid–Structure Interactions, Comput.Meths. Appl. Mech. Engrg. 1982, 33: 689-723.

14 C. Farhat, M. Lesoinne and N. Maman, Mixed Explicit/Implicit Time Integration of Coupled Aeroelastic Problems: Three-Field Formulation, Geometric Conservation and Distributed Solution, Internat. J. Numer. Meths. Fluids 1995, 21: 807-835.

15 R. K. Miller and A. N. Michel, Ordinary Differential Equations, Academic Press, 1982

16 Milton Abramowitz and Irene A. Stegun, Handbook of Mathematical Functions, Dover Publications Inc., 1965.

17 Roy R. Craig, Jr., Structural Dynamics: An Introduction to Computer Methods, John Wiley & Sons Inc., 1981.

18 Rick Lind and Marty Brenner, Flight Test Evaluation of Flutter Prediction Methods, American Institute of Aeronautics and Astronautics, 2002, AIAA-2002-1649.

19 Norman H. Zimmerman and Jason T. Weissenburger, Prediction of Flutter Onset Speed Based on Flight Testing at Subcritical Speeds, J. Aircraft, Vol. 1, No. 4, 1963.

20 Harold P. Van Cott and Robert G. Kinkade, Human Engineering Guide to Equipment Design, American Institutes for Research, Washington D.C., 1972.

21 Wesley E. Woodson, Human Factors Design Handbook, McGraw-Hill Book Company, 1981.

22 E. C. Levy, Complex Curve Fitting, IRE Transactions on Automatic Control, Vol AC 4, No. 1, pp 327, Dec 1958

23 C. K. Sanathanan and J. Koerner, Transfer Function Synthesis as a Ratio of Two Complex Polynomials, IEEE Transactions on Automatic Control, Vol. AC-8, No. 1, Jan. 1963.

24 Donald T. Ward and Thomas W. Strganac, Introduction to Flight Test Engineering, 2nd ed., Kendall/Hunt Publishing Company, 1998.

25 Henry A. Cole, Jr, On-Line Failure Detection and Damping Measurement of Aerospace Structures by Random Decrement Signatures, National Aeronautics and Space Administration, 1973.

26 Military Specification: Airplane Strength and Rigidity, Vibration, Flutter, and Divergence, MIL-A-8870B, 1987.

27 Interactive Analysis and Display System: Users Training – Basic, Symvionics, Inc, 1996-2003.

28 Bisplinghoff, R.L., Ashley, H. and Halfman, R.I., Aeroelasticity, Addison-Wesley Publishing Company, Menlo Park, California, 1955.

29 Fung, Y.C., An Introduction to the Theory of Elasticity, Dover Publications, New York, New York, 1969.

30 Van Nunen J.W.G. and Piazzoli G., Aeroelastic Flight Test Techniques and Instrumentation, AGARD-AG-160, Vol 9, ADA 065938, AGARD, London England, February 1979

31 Scanlan R.H. and Rosenbaum R., Introduction to the Study of Aircraft Vibration and Flutter, Dover Publications, New York, New York, 1968.

32 Stiltz, Harry L., Aerospace Telemetry, Prentice-Hall Incorporated, Englewood Cliffs, New Jersey, 1961.

33 Strock, O.J., Telemetry Computer Science, An Introduction 3rd ed., Instrument Society of America, 1983.

34 Doebelin, Ernest O., Measurement Systems: Application and Design, McGraw-Hill Book Company, New York, New York, 1983.

35 Skopinski, T.H., Aiken, William S., Jr. and Huston, Wilbur B, Calibration of Strain Gage Installations in Aircraft Structures for the Measurement of Flight Loads, NACA Report 1178, 1954.

36 Flutter Testing Techniques, NASA SP-415, 1976.

37 D.J. Ewins, Modal Testing: Theory and Practice, John Wiley and Sons Inc.,1984.

38 George F. Lang, Understanding Vibration Measurements, Application Note 9, Rockland Scientific Corp., December 1978.

39 R.K. Otnes and L. Enochson, Digital Time Series Analysis, John Wiley and Sons, 1972.

40 Haidl, G. and Steininger M., Excitation and Analysis Technique for Flutter Tests, AGARD Report No. 672. AGARD, London, England, January 1979.

41 Rabiner Lawrence R. and Gold Bernard, Theory and Application of Digital Signal Processing, Prentice-Hall Incorporated, Englewood Cliffs, New Jersey, 1975.

42 The Fundamentals of Signal Analysis, Application Note 243, Hewlett-Packard Company, Palo Alto, California, 1985.